SEGMENTATION OF HIGHLY CORRUPTED MEDICAL IMAGES

ALAN WILLIAM DOUGHERTY

PhD

The Hong Kong Polytechnic University
2019

The Hong Kong Polytechnic University

Department of Computing

Segmentation of Highly Corrupted Medical Images

Alan William Dougherty

A thesis submitted in partial fulfilment
of the requirements for the degree of
Doctor of Philosophy

September, 2018

CERTIFICATE OF ORIGINALITY

I hereby declare that this thesis is my own work and that, to the best of my knowledge and belief, it reproduces no material previously published or written, nor material that has been accepted for the award of any other degree or diploma, except where due acknowledgement has been made in the text.

_____ (Signed)

Alan William Dougherty (Name of student)

Abstract

Image segmentation is generally not straightforward and is still a fundamental problem in many fields, while there have been many different approaches to solve it, to date there is no definitive answer. While there is no generalised solution which can match human cognition, we can attempt to design algorithms which can work well for specific applications. In the case of medical imaging, there are a myriad of problems facing a successful segmentation algorithm depending on which particular problem it is being applied to. One such subset of this field is images with intensity inhomogeneities and corruptions. Although this is not a problem limited to the medical imaging, it does appear in many situations.

Another issue often faced in medical imaging when trying to create a fully automated system, is a lack of a reliable ground truth or "gold standard" to train the model. Moreover, even if one does exist there can often be some disagreement between different medical experts over the its validity. Unsupervised learning is less affected by this paradoxical dilemma, however, validating the results of these methods is slightly tricky and the evaluation of how well any such system is performing is not straight forward.

The focus of this research is on how to correctly segment and classify pixels in images which contain such inhomogeneities, as well as their classification for which-ever particular problem is being tackled. Three distinct applications are given, that of Multicolour-fluorescence in situ hybridization (M-FISH) imaging, retina blood vessel images and Magnetic resonance imaging (MRI). For each of these applications four methods will be presented.

First an investigation into how well an adaptive Kernelised Fuzzy C-Means

algorithm (FCM) can be used to segment pixels and also how the resultant output can be used intuitively in a Bayesian classifier. Specifically the research presented shows the results of the segmentation of M-FISH image data using a Kernel-based modified adaptive FCM algorithm; the kernel used was the Radial basis function exclusively. The research then shows how the responsibility values from the FCM algorithm can be used to form a set of probabilities for use in a Bayesian classifier, achieved by assuming that the intensity values of the constituent images are strongly correlated. To date the proposed algorithm has shown a vast improvement on the standard segmentation method.

Secondly, a method combining both pixel-wise and geometric-based segmentation methods could be used together to inform one another. The outcome was that by fusing together these two methods it was possible to get a better result than either used alone. Specifically looking at images at intensity inhomogeneities, some methods have tried to incorporate handling these into both region-based and geometric based, from this study it can be seen that by combining the two methods together they show a better result than individually

Finally, a method which fuses the benefits of both of the adaptive fuzzy algorithms and Level-sets if presented. Using the developments from both of the previous methods, a conditional energy formulation for a Level-set curve evolution is made by leveraging the uncertainties calculated from an adaptive FCM algorithm. This method shows a strong capability of overcoming the corruptions within M-FISH images with segmentation performance much higher than those it is compared with.

The proposed methods are verified using experimentation on public datasets and synthetic images. From the results it was seen that the proposed methods in this study can improve segmentation performance on small datasets of medical images which contain both inhomogeneities and corruptions which shows it has potential for use in real world applications of health informatics in the future.

Acknowledgements

I would like to thank my fellow doctoral students for their feedback, cooperation and of course friendship. In addition I would like to express my gratitude to the staff of the Department of Computing for their invaluable support. Most importantly my supervisor Prof. Jane You. Without all of her support and advice, none of this would have been possible. I am also grateful to Ms Mingzi Sun, a fellow PhD student for sharing her dissertation woes, and a glimmer of hope for post-thesis normalcy. Additionally, I would like to thank my friends for accepting nothing less than excellence from me. Last but not the least, I would like to thank my family for supporting me at every step throughout writing this thesis and my life in general.

Table of Contents

List of Figures

List of Tables

Abbreviations

CRF Conditional Random Field

MRF Markov Random Field

SVM Support Vector Machine

DTI diffusion tensor imaging

FCM Fuzzy C-Means algorithm

MRI Magnetic Resonance Imaging

M-FISH Multicolour-fluorescence in situ hybridization

RBF Radial Basis Function

Chapter 1

Introduction

1.1 Background

1.1.1 Current work

Images with intensity inhomogeneities present a real challenge when trying to segment them into specific regions, especially for applications where high accuracy is of a paramount importance i.e. medical imaging. It is well known that in the field of image segmentation that generally the neighbouring pixels in an image are highly correlated spatially thus if an image segmentation algorithm does not consider this fact it can result in numerous imperfections and spurious results. Magnetic Resonance Imaging (MRI) is one such field which suffers from this problem, and automated segmentation is an important quantitative tool for clinicians as an analytical tool as the qualitative analysis by experts is quite subjective.

Many algorithms use edge points to develop and estimate a modelled object contour. However, if is often the case that this is simply not sufficient to perform a correct segmentation of an image. Thus, it naturally makes sense to extend any of these methods to exploit other image properties. Some examples being spacial information and texture values which can provide invaluable knowledge about the image.

Literature shows the Fuzzy C-Means algorithm (FCM) is one of the most popular algorithms in various research fields of image segmentation. Comparing the FCM to hard segmentation methods, fuzzy clustering shows that it has a comparatively greater tolerance to image noise; this is in large due to the intrinsic properties of fuzzy set theory for taking into consideration the uncertainty of cluster membership for each pixel in the image. A prominent characteristic of many images is that its neighbouring pixels can often be highly correlated with neighbouring pixels and possess very similar feature values. Additionally, taking into consideration that the probability that these neighbouring pixels belong to the same cluster is relatively high, it is then plain to see that the spatial relationship is of great importance in clustering images. The standard FCM algorithm, unfortunately, does not utilise the spatial relationship between pixels, for this reason, much research has modified the objective function of the FCM algorithm to include a spatial constraint imposed on the centre pixel. The most common method for modifying the original FCM algorithm to take into consideration the spatial relationships is to alter its objective function. It is possible, for example, to augment the normalisation distance measurement and additional spacial terms can be added.

Importantly, even though other research has shown a high accuracy, there is also much need for the manual tuning of individual parameters during the ”automated” segmentation process, which is counter-productive towards any fully automated process. Thus more research needs to be completed in a move towards a fully automated system. Many existing fuzzy clustering methods also fail to take into consideration any a priori knowledge about the data set, even using data sets that do not have a reliable ground truth in order to use supervised methods, we can still conclude that having generated a set of responsibilities using the modified fuzzy clustering algorithm, we have indeed created a set of probabilistic values for each

pixel. Furthermore, there have been some methods which have also conducted a level of pre-computation before clustering, such that they have adapted the image to its own inhomogeneities so that the clustering process had become more accurate.

1.1.2 Current problems

Images with noise, artefacts and inhomogeneities remain to be a major issue in image segmentation, while there are may different algorithms and approaches which have been designed, it remains a fundamental problem in computer vision and image processing. When looking specifically at the application of fuzzy set theory towards multi-layered image processing current methods do not take advantage of the existing correlated probabilities between the layers. This leveraging of probabilities makes fuzzy-based algorithms potentially a highly effective method for multi-spectral imaging. It is the intention of this research to investigate the effectiveness of fuzzy clustering methods at performing segmentation by leveraging the correlated probabilities from multiple responsibility values. In addition, there seems to be a gap in the current research for applying kernel-based FCM methods to MRI image data. It turns out the calculation of a probabilistic classifier using multiple layered responsibilities is computationally simpler when using the Kernel-based FCM. Thus it seems to be a natural direction for the research to take.

We can take two distinct examples which contain similar problems. Firstly the Multicolour-fluorescence in situ hybridization (M-FISH) karyotyping image segmentation. The finer points of this method are discussed later in section 3.1, the important factor is that the result of the imaging process leads to an uneven distribution of intensity values, this is often called the gain field [1]. Secondly, MRI imaging has a problem caused by the so called bias-field [2]. While much work has already been conducted and proved the importance of spatial constraints being imposed on the objective function of the FCM algorithm, there still remains to

be investigated the application of Kernel methods being applied to these spatially constrained equations. Furthermore the resultant membership functions have an untapped potential when dealing with these types of datasets, from the currently completed work it will be shown that it is possible to vastly improve the classification accuracy by considering the membership functions from each of the layers in the M-FISH image as part of the same probabilistic problem.

1.1.3 Research goals

To solve the problem of segmenting images in the medical imaging realm and given the discussed issues of the inhomogeneities and artefacts existing, this research will pose the following questions:

1. When imposing the spatial constraint of the object function of a fuzzy clustering algorithm, which spatial and size works best for medical images with intensity inhomogeneities?

2. Projecting the extracted intensity features to a higher dimensional space using Kernel functions, is it better to use one single Kernel type or multiple, and which will give the best performance?

3. Can the spacial information and derived pixel uncertainties from the FCM algorithm be leveraged into geometric based methods such as the level-set function?

1.1.4 Significance of the work

Early diagnosis of tumours or genetic anomalies can vastly improve the number of possible treatments as well as survival rate from potentially fatal conditions. Moreover, the application of most brain tumour therapies can be potentially harmful if incorrectly guided, so it is of paramount importance that a tumour is segmented

accurately in order to safeguard the healthy tissue. This process is lengthy and involves various steps[3]. Importantly, the standard clinical process implemented at this time, involves the manual annotation of extremely large datasets; This process is time consuming and expensive. In comparison to other methods such as deep learning, fuzzy clustering is computationally inexpensive and is highly explainable in how it behaves. This is one feature which is important for medical image processing, as ultimately it is potentially life threatening if something goes wrong and one of the biggest problems facing any automated system is the adoption and faith given by the medical community. The development of a robust, computationally inexpensive, explainable and accurate segmentation algorithm is highly significant. The research proposed to tackle these problems and produced a novel kernel-based adaptive algorithm which can compensate for intensity inhomogeneities while leveraging the internal probabilities to improve the classification accuracy. The research also proposed a hybrid clustering-level set method which used the output of a kernel-based fuzzy C-means algorithm into an active contours algorithm to regulate normally smooth boundaries of the segmented objects. Finally, the research proposed an active contours method based on a modified Chan-Vese variational level set algorithm which leveraged the probabilistic uncertainties from a kernel-based fuzzy C-means algorithm as input.

In the case of level sets, this is a numerical method used for finding and tracking interfaces, where the zero level set of a projected higher-dimensional function is representative of the target object contours. Due to the robust numerical nature, the level set method is advantageous because it is an already well-established set of mathematical tools as well as not requiring parameterisation and can represent complex topologies. However, there are some issues facing certain types of level set algorithms. For example, many are based on piece-wise models or edge based

models, whilst they do not have any assumptions of image intensity homogeneity they rely heavily on correct initialisation and also need strong object boundaries.

1.2 Thesis Structure

This thesis consists of 7 chapters and contain as follows:

Chapter 1 Contains an introduction and background to the investigated problem.

Chapter 2 Contains a literature review of all of the topics investigated and their related backgrounds

Chapter 3 Contains a description and important information on the real work dataset used.

Chapter 4 Describes the development of a novel kernel based fuzzy C-means algorithm applied to the M-Fish karotyping dataset.

Chapter 5 Describes the method and experiments carried out on a hybrid clustering and level set method.

Chapter 6 Describes the final method which fuses all of the previous methods to create a fuzzy region based level set algorithm. This is then tested on the real world M-Fish dataset.

Chapter 7 Presents conclusions and discussions of the overall work.

Chapter 2

Literature Review

2.1 MRI imaging

Brain imaging has wide-ranging applications, from trying to better understand how human cognition functions, to treating brain tumours. With these applications, each is of vital importance to future development in their respective fields. Although brain tumours account for around only 1% of all cancers, they are still the most fatal. Improper treatment can lead to incredibly life-altering consequences such as paralysis or loss of certain cognitive abilities. Proper detection and identification of diseased regions is of vital importance to ensure patient safety and survival rates.

The examination of brain tumours for treatment is achieved via brain imaging, usually using the medium of MRI data; although there are a few other methods each with their own merit. In fact, MRI analysis of brain images for the study of tumours is gaining increasing interest in research recently, due in part to the need for an objective, efficient, automated system which can handle large volumes of data. The issue facing brain imaging are multi-faceted, manually segmenting the images is incredibly costly and time-consuming and generally even amongst experts in the field there are relatively large discrepancies within their decisions of how to segment and identify regions of interest. In addition to this, there is the issue of

the deformable morphology of the brain, especially in the case of tumour growth or shrinkage during various stages of treatment.

The role of machine intelligence and image processing in tackling these issues within the treatment of these cancers is of great importance. Algorithmic automatic detection of the regions of interest can drastically reduce the amount of time spent by experts manually segmenting images and also potentially increasing the survival rates of patients, giving both a medical and economic incentive. However, there are many difficulties in designing such a system to perform this task. As mentioned earlier the inconsistencies in the analysis by experts as well as the issues revolving around image registration of a deformable object.

Developing a robust manually updatable automated segmentation framework has several advantages. By utilising an automated algorithm, it removes workload from clinicians saving them vast amounts of time, and allowing the clinicians to then manually tweak this data will then ensure a higher level of accuracy. With this increased accuracy, there is the possibility that the Doctor's faith in the algorithm will increase, helping to solve the major issue of lack of implementation of such systems. By collecting these manual updates, priors in the decision algorithm can be updated with new corrections to the predictions.

One of the key issues facing the correct segmentation of MRIs is the existence of Intensity inhomogeneities or the so-called bias field caused by the inherent nature of the image acquisition method or those introduced by movement of the patient. These imperfections or artefacts can cause serious problems to automated segmentation algorithms. In an attempt to automate the process of segmentation many different methods have been attempted, region based, edge based, classification based and clustering based are such examples. Each method has shown its own comparative successes however still there does not exist a solution which is robust

enough to solve the problem of MRI segmentation.

In MRI, the pixel intensity values tend to have a problem where they are corrupted by the so called "bias field", this is a gradually varying noise which affects the whole image in a gradient like effect. While Meyer et al. had predicted that approximately 30% of all the pixel intensity values are affected by these inhomogeneities there is no sure way to know to what extent they have been corrupted[4].

It is important to know exactly what the bias field is doing to the intensity values, in general it can be seen that it will unevenly distribute the intensity values around some local regions. Overall the effect will be such that the central regions will have a much higher average intensity that those in the outer regions of the brain image; although this may not affect an expert human observer to a great degree, it will cause an automated algorithm many problems. To overcome this problem there has been much research carried out to estimate the bias field[1, 2, 5–12]. These works include methods such as histogram based methods[10], estimation with the EM-algorithm[11, 12], with most of the work attempting to somehow model the bias field as a relationship between each pixel and its immediate spatial neighbourhood[1, 2, 5, 7] using fuzzy clustering. As Nabizadeh and Kubat points out in their work using wavelets, traditional clustering methods do not work well with brain image segmentation due to their inability to deal with inhomogeneities. However, because of the success of fuzzy methods in handling the uncertainty introduced by the inhomogeneities and artefacts, much research has focussed on these methods in recent years.

As shown by Bauer et al. most segmentation architectures can be broken down into similar pipelines[14]. Concentrating on the segmentation part of the pipeline, it is important to determine which sort of features will be used for the segmentation algorithm. Bauer et al. break the current trend for segmentation algorithms into two

main groups, region/edge based and classification/clustering based.

2.2 Feature extraction

It is important to establish which features to use in the algorithm to be developed, for medical images the typical feature used is pixel intensity values, other features include alignment based and texture based[15, 16]. It is often possible to take advantage of the inherent structural elements of the brain such as the symmetrical nature of the left and right hemispheres, and the shape estimation of the tumour can be achieved using edge-based methods by this comparison of the symmetry[17, 18]. Recently there has been much interest in multi-modal and feature fusion strategies. We can observe that there has been much interest in how different features can improve the performance, for example[19], showed that combining features gave a significant performance boost and[20] showed that by combining texture, shape and intensity values they could achieve a much higher accuracy for multi-modal images. Overall, almost all of the research uses image intensity values as a feature, based on the general assumption that brain tumour tissues exhibit a different greyscale intensity values compared to the surrounding healthy tissues.

2.3 Image segmentation

2.3.1 Edge-based

The brain and brain tumours can be modelled as a deformable objects[21–23], and certainly when trying to solve the issue of image registration there has been much success with this form of model.

These deformable models are successful by using edge detection and registering the local elements of the images[24]. In general, the edge-based methods are achieved by growing a level-set on the voxels to find the tumour boundaries.

Other methods include vector-flow models as used in[22] and region-competition level-set[25]. Ho et al. achieved the region-competition method by forming a tumour probability map by comparing various image types i.e. T1 and T1c images. Similarly[26] used a region-growing approach to form a map of tumour likelihoods, and[27] developed a region-based fuzzy-connectedness algorithm. Importantly the work in[27] did not take into consideration the spatial information of the MRI image.

2.3.2 Clustering/Classification based

To date, the most common form of brain tumour segmentation algorithms utilise clustering or classification methods. Clustering and classification, do of course differ in the fact that classification methods require training whereas clustering can work as an unsupervised method. Due to the fact that there is a variability in ground-truths and MRI imaging is multimodal which are both situations which can be easily handled by these methods. As mentioned earlier, mostly these will utilise the intensity values or texture information as a feature, processed voxel-wise.

Looking at how clustering was introduced into applications to brain tumour segmentation, it was initially the work in[28] which used clustering to analyse the texture values in various tissues, from here the FCM algorithm was used in[29] and later by[30] for it's comparison to the KNN algorithm when determining the tumour volume. This was later expanded to work with knowledge-based methods in[31] and[32] fused these methods for use in brain tumour segmentation. These methods still did not incorporate the spatial data.

There have since been many developments not only in classification methods but also in how complicated the classification performed is. For example the works in[33] and[34] used an increased level of modality by incorporating diffusion tensor imaging (DTI) channels to the standard MRI channels which were then classified

using Support Vector Machine (SVM); this was able to not segment various levels of healthy and necrotic tissues into multiple levels of tumour severity. Another method which used SVMs but with a lower modality is the work in[35], this also proved to be effective but the lack of higher modality also reduced the complexity of the segmentation. This work was further developed using the Kernel trick in SVMs and showed that it could improve the results[36]. Finally, there has also been much work using other methods such and ANN's[37] and decision trees[38].

2.3.3 Classification and clustering with additional constraints

Taking into consideration that the most common feature used in MRI image segmentation is voxel intensity values, it can be said that by simply using this, it does not take into consideration all of the available information. This is indeed true for other fields of general image segmentation and also other forms of medical image segmentation i.e. the aforementioned M-FISH image segmentation. Because of this there has been much research carried out to attempt to incorporate additional data available within the images to improve the results of the segmentation. This is usually achieved by enforcing additional constraints on the learning model such as local neighbour pixel values, shape information or for the specific example of tumour segmentation, the location of the tumour within the brain could be constrained. The latter point can be achieved using the so-called Atlases. These will now be discussed in more detail.

Brain Atlases can be used to impose prior knowledge on a classification problem or creating generative classification models. They contain very detailed prior knowledge of brain structures and topology of certain diseases. For example, the KNN algorithm was used as a classifier by[39] using the spatial information from a brain Atlas to inform their "adaptive template-moderated classification algorithm". Not only has spatial information has been incorporated using Atlases but

also the prior knowledge of tissue information, the work in[40] and[41] created a probabilistic-based tissue model using the EM-algorithm. This leveraged the tumour location data from a brain Atlas and augmented the Atlas with specific data from patients about their tumour using various image modalities. Finally, the spatial relationships from neighbouring voxel data is often achieved post-classification using Markov Random Field (MRF) or Conditional Random Field (CRF)[42, 43].

From here we can draw some conclusions, firstly, the neighbouring voxel data is of great importance to correct segmentation. Secondly, traditionally clustering methods do not take into account this information. Finally, Fuzzy clustering methods are effective at handling images with inhomogeneities.

2.4 System Evaluation

When implementing any system it is important to know how evaluate the success of it, because we want to eventually apply the system to the segmentation of brain tumours, the following section will examine how to evaluate such systems. For tumour prognosis, the volume of the necrotic tissue is the key measurement for successful treatment[44]. When dealing with manual labelling, the nature of the task and its difficulties leads to much variability in the results of approximately 80%. Some of the difficulties faced by oncologists when trying to segment brain tumour images include: trying to label data form a 3D data set by observing 2D images, the variability between intensity statistics across different MRI images and also the tumour often lacking well-defined edges. The other side of this problem is that automating this process is also a challenging task, leading automated systems not making it into clinical use[45]. These are problems faced by most image segmentation algorithms, but they are also compounded by the nature of the brain and tumours themselves. The lack of clear boundaries between normal and necrotic tissue as well

as the changing morphology of the brain as the tumour progresses[46] cause major issues to any automated system; the great variation in tumour size and shape and their having intensities which can overlap into healthy tissues mean that many traditional image segmentation methodologies are not suitable for the task[47]. With many automated segmentation systems not meeting prognostic needs[44] and failing with certain cases, the lack of robustness leads to a lack of Doctor faith in them.

This lack of robustness and the fact that ultimately the buck stops with the clinician, has led to recent literature proposing semi-automated or interactive segmentation systems. The problem faced by many of these, as pointed out by[45] is they lack the control desired by the clinician. To tackle the issue of lack of robustness and control: Some authors have suggested the idea of a semi-automatic segmentation

There is several very similar examples of semi-automated segmentation [44–46], with a marked exception of the method used in Bauer et al.. Instead of a user defining areas for segmentation and the algorithm then automating the process by methods such as graph cuts etc. and then propagating this data into 3D volumes, the system fully automates the segmentation, and the clinician can then alter the results as needed after the fact. This has a major advantage over previous methods where the system is just fully automated, not only for the obvious reasons where the robustness is improved by having clinicians making the segmentations decisions themselves but also in terms of gaining invaluable statistical data on how the algorithms were incorrect; long term this can help improve clinician trust in the automated process.

To move forward from this previous research, work needs to be done to tackle the issues around robustness by combining fully automated segmentation and clinician updates, with state of the art machine learning techniques. While brain imaging

is a very broad field, we can concentrate on one particular application, brain tumour segmentation and observe where the major pitfalls are in the current research. Much research focuses on a human-centric approach of 2D image analysis and extending this into 3D data rather than considering the data as-is.

Also, these methods which use automated segmentation with manual updates, do not feed these updated "ground truths" back into the learning algorithms as updated priors, however doing so would create another problem, wherein the aforementioned lack of concordance in how to segment the images by experts would lead to multiple ground truths. Thus it can be seen that this naturally leads to a separate clustering of classifiers from different sources to attempt to bring back a level of objectivity only found in a fully automated system.

Thus it can be seen that an unsupervised method which can be validated by experts is ideal for brain tumour segmentation, as while it does not rely on the expert knowledge to gain an initial result but it can have those results improved by validation from the expert. Furthermore it has been noted that using kernels to assist the classification of tumours could be highly effective.

This leads to the design of the semi-automated segmentation branch of the research. Methods for updating the results should be investigated. These require human interaction and thus eventually they must be tested with real users, preferably, on expert users.

Evaluation of any imaging system is difficult, as there is no set ground truth that is widely accepted. Thus as Bauer et al. states, the current gold standard for evaluation is to compare with expert results, but as pointed out already this is not only a tedious task but also subject to a lack of concordance between experts, seeing variability of approximately 20-30%[50]. Because we have initially proposed to use the BRATS dataset, this can be used as a ground truth for evaluation. However, for

future purposes and development, this would not be ideal.

Chapter 3

Multicolour fluorescence in-situ hybridization images

When investigating the segmentation of MRI data, there are often parallels shown between the gain field found within M-FISH images and MRI data. For instance, the work by Pham and Prince, started as a segmentation algorithm for M-FISH image data and was then developed into one for MRI data. By using this as an inspiration, the current work has used the same process to inform its development. Following this incremental style allows for the development of an algorithm to segment non-homogeneous 2-D-images and later develop the algorithm into the 3-D domain. Furthermore, because the M-FISH image data-set consists of multi-channel 2-D images which often presents severe non-homogeneous pixel intensities, it would allow for the development of an algorithm which can deal with multi-dimensional problems as well as segmenting images which contain corruptions. The following section discusses contemporary methods used on M-FISH image data. Further to this, there will be a discussion of the links between existing methods and the research presented in this thesis.

3.1 Non-homogeneous image segmentation

3.1.1 Background

A multitude of medical and health problems can be detected by analysing human chromosomes, but to achieve this, it requires that clinicians image cells and separate each of the 46 chromosomes of the cell into 22 pairs of autosomes and the sex chromosomes. This method of imaging and then grouping chromosome into pairs is a clinical process known as Karyotyping. Using these Karyotypes, geneticists must use their expert domain knowledge painstakingly segment the images manually so that the pixels can be classified into 23 or 24 chromosome classes. M-FISH imaging is a technique which uses different coloured dyes to stain the chromosomes such that only specific pairs of chromosomes absord a particular dye and then will fluoresce when excited by a specific wavelength of light. After imaging, a combinatorial labelling technique is used by tracking the chromosomes fluorescent response to each wavelength of light and then labelling it as either one or zero; the M-FISH technique will utilise six different wavelengths also known as channels. Additionally, the chromosomes are stained with the DNA dye 4-6-diamidino-2-phenylindole (DAPI) which will attach to all chromosomes i.e. all chromosomes will fluoresce[51, 52]. The result of this imaging process is that pixels belonging to a particular chromosome will exhibit a higher intensity than others when excited by the correct wavelength, allowing for them to be visually classified by a human observer.

While it is true that the newer process of M-FISH imaging has made creating karyotypes simpler, there is still a great need for a reliable automated system. To achieve the aim of a fully automated system, there are currently two main branches of medical imaging research focussed on M-FISH images: Region based classification[53–60] and pixel-wise classification[54, 61–63]. This work will be

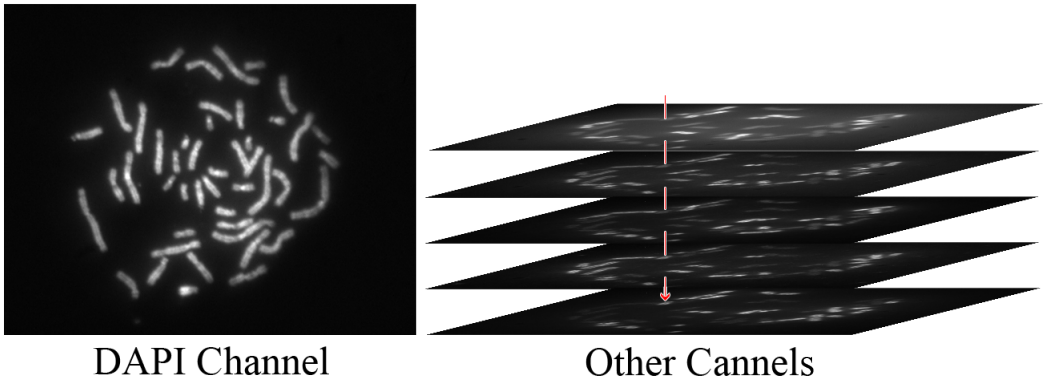

Figure 3.1: An example of one M-FISH image, showing the 6 channels.

initially focusing on pixel-wise methods and then hybridised with geometric methods. The highest success rate Pixel-wise classification algorithms, generally work by initially segmenting the chromosome pixels from the background pixels. Background segmentation is almost always achieved using the intensity response to the DAPI channel. The remaining channels use the result of the DAPI channel to remove their background pixels and are then used to classify the pixels into their corresponding classes. The chromosome classes are defined by using the combinatorial labelling technique for M-FISH karyotyping found in Speicher et al.. Figure 3.1 shows one such example image: The DAPI channel has fluoresced for all chromosomes and highlighted with the red arrow showing whether pixels on the other channels have fluoresced or not.

Traditionally this process is performed manually by trained experts, but it remains too time-consuming and laborious; thus, there is still a need for an automated system to complete this task. However, there are numerous issues facing the automation. As with many fields of medical diagnosis, there is generally a problem of inter-expert variability, meaning that obtaining a reliable ground truth is not always possible. Moreover, M-FISH images by large contain many inhomogeneities/unevenly distributed pixel intensities and image artefacts.

Table 3.1: Combinational logic table for the M-FISH image set.

	Channel label					
Chromosome #	DAPI	Aqua	Green	Gold	Red	Far Red
1	1	0	0	1	0	0
2	1	0	0	0	1	0
3	1	1	0	0	0	0
4	1	0	1	0	1	0
5	1	0	0	1	0	1
6	1	0	1	0	0	0
7	1	0	0	0	0	1
8	1	0	0	0	1	1
9	1	0	0	1	1	0
10	1	1	0	1	0	1
11	1	1	0	0	1	0
12	1	0	1	1	0	0
13	1	1	1	0	0	0
14	1	0	1	1	1	0
15	1	1	0	1	1	0
16	1	0	1	0	0	1
17	1	0	1	0	1	1
18	1	0	0	1	1	1
19	1	0	1	1	0	1
20	1	1	1	0	1	1

3.1.2 Channel selection

Because the M-FISH image set is a multi-spectral image set we first need to be clear about the channel selection used. All of the classification methods for determining which pixels can be considered correctly segmented can be shown using a combinatorial logic table shown in table 3.1 on page 20. For example, if we wish to classify a pixel as chromosome 1, then the segmentation algorithm would need to output a one on both the DAPI channel and the Red channel. If we wanted to classify a pixel as chromosome 10, then the segmentation algorithm would need to output a one on both the DAPI channel, the Aqua channel and the Gold channel.

3.1.3 Noise Model

To properly align any segmentation algorithm with the chosen dataset, we must first understand the nature of what type of noise and corruptions exist within the dataset. As such, information on some of the noise model of M-FISH karyotyping dataset which is used is as follows.

Image acquisition: These are errors introduced by the image acquisition process; for instance, by the microscope used to capture the images. Due to the nature of the optical image process used, there exists an intensity bias across the image such that the centre of the image is often much brighter than the surrounding image. The chosen algorithm would have to be able to incorporate this bias field into the noise model used in the segmentation process.

Flare effects: The chromosome/background boundary tends to have a much denser intensity distribution than that of the background pixels far away from the chromosome. Causally, the pixels at the centre of the chromosome will also be much lower than those surrounding it. This uneven intensity distribution can result in background pixels being incorrectly classified as object and object pixels being incorrectly classified as background. Thus, the chosen algorithm needs to be able to adapt to the flare effect in the noise model.

Uneven dye-distribution/hybridisation: Because the hybridisation process is not perfect, there may be situations where the dye used in the staining process is not even, causing the intensity of the chromosome pixels to vary a lot, i.e. have lot amounts of intensity inhomogeneity which can significantly affect the classification accuracy.

3.1.4 Fuzzy Models

Because it is often the case that medical imaging has imprecise or incomplete information Fuzzy set theory can be of great use, due to its inherent ability to deal with

these unknown or unclear distributions. This section will clearly define why fuzzy methods are chosen for dealing with M-FISH image data.

Image information representation: the information within an image can be represented at differing localities by fuzzy sets, i.e. local or global pixel information. Thus, we can use both the local pixel intensities while maintaining a spatial constraint. Maintaining this allows the algorithm to overcome issues such as the global bias introduced by the image acquisition process.

Uneven data-distributions: it is quite common when dealing with medical image sets that the data-distribution could be quite uneven. This issue is especially the case with M-FISH image sets, as not only the distributions of the background to foreground images is extremely uneven but it can also vary between the spectra (channel) of each image in the set. For example, the DAPI channel may have a relatively even distribution, but the Gold channel may be very uneven. Fuzzy models are very effective at dealing with overlapping and uneven decision boundaries. Thus, they can make an effective method for M-FISH image sets.

The Fuzzy C-means algorithm has a strong ability to take advantage of the previously mentioned attributes of fuzzy models to overcome to issues listed in the noise model of M-FISH karyotyping images.

Chapter 4

Method 1: Kernel-based Adaptive Fuzzy c-means algorithm

4.1 Overview

There are many different methods available for use in medical image segmentation, so it can be a challenging task to pick a suitable method for each target problem and dataset. As mentioned previously in chapter 3, the main dataset used in this Thesis contains a lot of unpredictable corruptions, which are hard to model.

Because performing segmentation on images with intensity inhomogeneities is such a challenge especially for applications such as medical imaging, where extremely high accuracy is needed, there is a strong need to correctly understand the problem domain before attempting to implement any algorithms. As the neighbouring pixels in a medical image are often highly correlated spatially, the image segmentation algorithm must consider this fact; otherwise, it can result in fatal imperfections and unacceptable results.

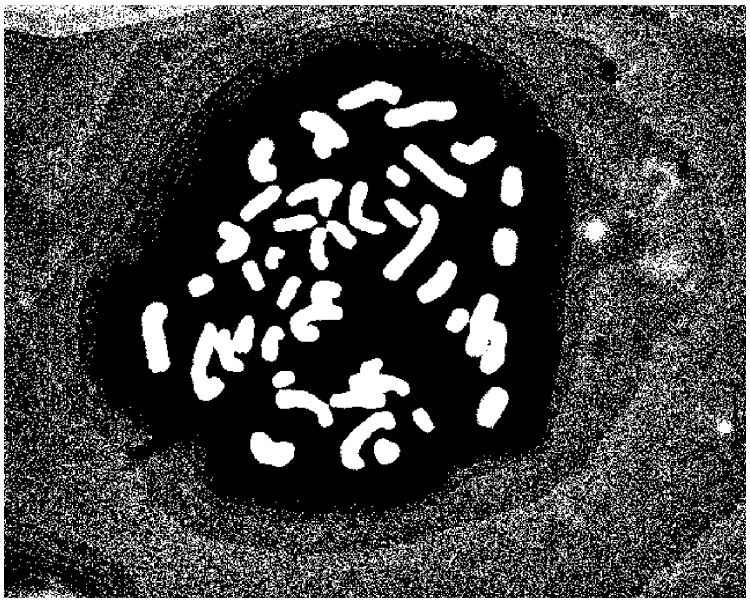

Figure 4.1: Result of segmentation using non-spatial algorithms

4.1.1 Traditional Methods

Figure 4.1 shows the result of segmenting the DAPI channel using some of the MATLAB tool-boxes, in this example it is specifically using thresholding which does not take into account the spatial relationship. Because of the lack of spatial data the surrounding background and its artefacts and noise have been incorrectly segmented as chromosome pixels.

4.1.2 Fuzzy clustering

Because of the FCM algorithms is an unsupervised method with a strong ability to tolerate noise within an image when comparing it to hard segmentation methods, the use of FCM within various fields of image segmentation where the datasets are relatively small is quite noticeable. The ability to handle noise is due in part to the inherent nature of Fuzzy set theory which takes into consideration the uncertainty of cluster membership for each pixel. However, this is often not enough for every dataset and given that one of the prominent characteristics of many images is that neighbouring pixels can be highly correlated and that pixels possess simi-

lar feature values it is prudent to take this into consideration. The probability that these neighbouring pixels belong to the same cluster is high, so it becomes evident that the spatial relationship is highly important in image segmentation when using clustering. As mentioned before the standard FCM algorithm does not take into consideration this spatial relationship, thus many researchers have modified the objective function of the FCM algorithm to have a spatial constraint focussed around a central pixel.

However, the basic FCM algorithm and many of its derivatives utilise the L_2 norm distance metric in order to determine the locality of the data points in relation to one another; it could argued that this does consider some of the spatial information it but is extremely limited. While being useful for spherical clusters[64, 65], it does not perform well for data which has more complicated configurations. Many fuzzy clustering algorithms with spatial constraints work well with standard noise models but they are not as effective with the inhomogeneities found in many medical imaging problems due to their limited adaptation to the spatial information; the spatial constraint performs better if it is designed to adapt to the pixels in terms of their relationships local to one another.

When performing ”defuzzification” or segmentation on the output of any fuzzy clustering algorithm which has been applied to an image, the typical method is to approach it from a hard, winner takes all perspective. However, in the method proposed in this chapter we consider it from a more probabilistic standpoint. By using the proposed algorithms output, we use the derived responsibilities from the fuzzy clustering algorithm as an intrinsic probabilistic variable representing the level of certainty, that the corresponding pixel belongs to a particular chromosome pixel class. The current state of the art classification rate for M-FISH images is still not high enough for clinical applications. As such, additional research is required with

a focus on a high ratio of accurate classification of pixels as chromosomes (CR) and a low misclassification of chromosomes as background pixels or false detection rate (FR). CR and FR are defined by eq. (4.1).

$$CR = \frac{\text{Number of chromosome pixels segmented correctly}}{\text{Total number of Chromosomes}}$$
$$FR = \frac{\text{Number of background pixels segmented as chromosome pixels}}{\text{Total number of Chromosomes}} \tag{4.1}$$

To solve this problem, we have developed a system using a pixel-centric adaptive spatial constraint on the objective function combined with kernel methods to project the data into a higher dimensional feature space. This projection into a higher dimensional feature space combined with an adaptive spatial constraint allows for more accurate separation of the clusters[66–69].

This chapter will present a novel application of this theory, utilising both fuzzy clustering with spatial constraints and applying the kernel trick to more accurately model the uncertain cluster membership and a probabilistic defuzzification method with the aim of improving the classification of chromosome abnormalities in M-FISH karyotyping.

4.2 Methodology

Recent research shows that the use of various flavours of a modified FCM [8, 58, 70–73] is currently a popular method is for using the spatial information to account for the problems faced in segmenting images with intensity inhomogeneities. Looking at the basic FCM, although it is better than using hard clustering at segmenting non-homogeneous images it does not take advantage of the strong correlation that exists between the neighbouring pixels that can be found within

many medical imaging problems. Similar to all image segmentation methods, the implemented algorithm needs to group the image pixels into various class spaces. When we are dealing with M-FISH image segmentation, we are tasked with isolating the chromosome space from non-chromosome space. Thus our proposed method, with an aim to change the vanilla FCM algorithm, needs to minimise over a cost function which includes this important spatial information. Being analogous to the FCM membership function, this spatial function should also be representative of the probability that some i^{th} pixel in the image belongs to the k^{th} cluster[8]. Additionally, there are algorithms which have used both local and non-local spatial constraints. Such local and non-local spatial constraints are advantageous as other methods only using a local spatial window are more susceptible to noise[74].

To change the basic FCM algorithm to take into consideration the spatial relationships we need to modify its objective function. Equation (4.2) shows the unmodified objective function of the FCM algorithm; this unmodified version does not consider any of the spatial characteristics of the data. Where $u_{k|i,j}$ is the membership function of the $(i,j)^{th}$ pixel to the k^{th} cluster centroid. $d(y_{i,j},c_k)^2$ is a distance metric, typically the L_2 norm although it is possible to use others such as Mahalanobis distance[75].

$$\begin{aligned} J_{FCM} &= \sum_{i=1}^{N}\sum_{j=1}^{M}\sum_{k=1}^{\Omega} u_{k|i,j}^{p} d(y_{i,j},c_k)^2 \\ &\text{s.t} \sum_{k=1}^{\Omega} u_{i,k} = 1 \ , \ u_{i,k} \in [0.1] \end{aligned} \tag{4.2}$$

Equation (4.3) and eq. (4.4) give an example of prototypical a modified object function and one example implementation, respectively; eq. (4.4) is the IAFCM from Cao et al., where a normalisation distance measurement and additional spatial terms are considered. Equation (4.4) can be utilised as a template for solving

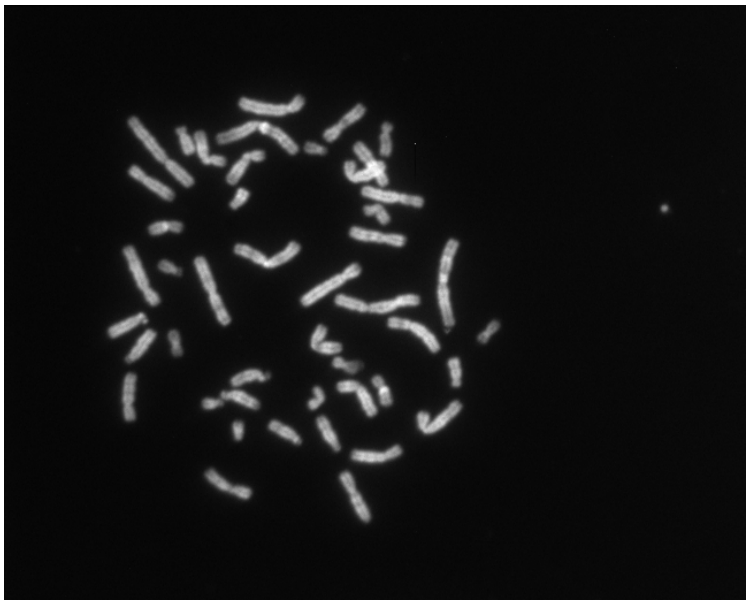

Figure 4.2: Sample Karyotype image

the generalised problem of non-homogeneous image segmentation; such a template does, however, need changing to suit the target problem.

$$\begin{aligned} J = &\sum_{i=1}^{N}\sum_{j=1}^{M}\sum_{k=1}^{N_c} u_{k|i,j}^{p}\hat{d}(y_{i,j},c_k) \\ &+\lambda\sum_{i=1}^{N}\sum_{j=1}^{M}\sum_{k=1}^{N_c} u_{k|i,j}^{p}\sum_{r\varepsilon D_r} G_r \end{aligned} \tag{4.3}$$

$$J_{IAFCM} = \sum_{i\in D}\sum_{k=1}^{N_c} u_{ik}^{p}\,\|y_i - g_i C_k\|^2 + \lambda\sum_{i\varepsilon D}(g_i - (g*H)_i)^2 \tag{4.4}$$

For various fields of research, the correlation between any single data point in a vector and its corresponding neighbouring data points is important. For clustering techniques, the spatial correlation between any one data point in the clusters can be seen as highly important to the model's structure; thus there is a strong motivation to consider this structure when designing a clustering algorithm.

Hard clustering methods have traditionally assumed that each datum in the data-set would entirely belong to a single class. As such, often times there can be a

case where a data point lay on the border of two neighbouring but disjoint classes but is classified with 100% certainty that it belongs to one of the classes. Moreover, the uncertainty of which class the datum belongs to could be influenced by missing data, corruption in the data or due to the inerrant lossy nature found in data collection methods. For certain situations where the data-set has very well defined and has disjoint groups of data, hard clustering can be considered as suitable. However, for many real-world datasets, this is most likely applicable. For example, the procedure for M-FISH image segmentation is to initially separate pixels of interest from the background. In this two-class problem, one could naturally assume, that if the target pixels have a much higher intensity than those of the surrounding background pixels (as shown in fig. 4.2), then a hard clustering algorithm would be relatively effective.

However, in reality, many of the pixels, specifically those at the boundaries of the chromosomes object would be incorrectly clustered; in general, there can be a certain degree of uncertainty around object edges in images. This uncertainty at the edges of objects is especially true when the image exhibits a poor resolution, or the objects are poorly defined. The uncertainty of object boundaries is a typical example of clusters overlapping, and of how data points can belong partially to multiple clusters. Thus for any clustering algorithm work effectively, it has to consider the uncertainty between groups of data within a set. Fortunately, Fuzzy set theory can be applied to clustering techniques, using the innate properties of Fuzzy set theory it is possible to resolve this issue by incorporating a model of the uncertainty of cluster membership.

4.2.1 The FCM algorithm

The original FCM algorithm remains relatively sensitive to noise which can lead information loss at the boundaries of an object, or in other words, there is a high uncertainty at an object's edge. This problem is also often alleviated using a spa-

tial averaging algorithm, such algorithms will be discussed further. One of the prominent characteristics of an image is that neighbouring pixels can be highly correlated/neighbouring pixels possess similar feature values, and the probability that these neighbouring pixels belong to the same object is significantly high. It is then evident that the spatial relationship of pixels is essential in clustering images. The original FCM algorithm does not consider this spatial relationship. Thus, there is much research which has modified the objective function of the FCM algorithm to include a spatial constraint imposed on the centre pixel[72, 76, 77]. This approach to modify the objective function of the FCM algorithm to enhance its ability to cluster the data correctly has been taken by much research.

Equation (4.2) shows the unmodified object function of the FCM algorithm, where M and N are the horizontal and vertical indices of the image respectively, Ω is the number of clusters, $u_{k|i,j}$ are the cluster responsibilities for each data point/pixel with a fuzziness factor of p and the function $d(y_{i,j}, c_k)^2$ is some normalising distance function between the current data point $y_{i,j}$ and the predicted cluster centroid c_k; in common practice $d(y_{i,j}, c_k)^2$ is the L_2 euclidean norm.

Next we will discuss the various methods for incorporating spacial constraint.

4.2.2 Spacial constraints

Following from the previous section, the spatial constraints imposed on the objective function requires much attention, there are many examples of algorithms using a weighting function on an additional spatial averaging term[58, 78, 79] in the optimisation function. Using methods such as gain fields[1, 2, 7, 70] it is possible to put a higher weighting to pixels with more neighbouring pixels, with the gain factor acting as an amplifier using the averaging convolutional kernel[7] as shown in eq. (4.4).

Cao et al. further developed the adaptive spatial constraint FCM (AFCM) algorithm by Pham and Prince using gain-fields of different shapes to better compensate for the particular properties of intensity inhomogeneities in M-FISH image. This improved adaptive FCM (IAFCM) showed a significantly better performance than their previous method. One of the main advantages exhibited by the IAFCM algorithm is its apparent capability to adapt effectively to local image inhomogeneities.

Cao et al.'s proposed gain-field gave a cumulative bias to pixels whose neighbouring pixels had a higher intensity value, unlike global gain fields or global averaging, it also considered the local inhomogeneities[7]. However, the fact remains that the algorithms classification accuracy is still too low for use in clinical applications. Thus, further investigation and algorithmic development are still needed when using local pixel intensity biasing in M-FISH chromosome classification.

Another advantageous property of the IAFCM algorithm is that it also uses the cluster centroids during the pixel amplification process. When performing fuzzy clustering, we are more interested in calculating the membership function for each pixel rather than the calculated cluster centroids; thus it is perfectly reasonable to do this. This realisation that cluster centroid values are not entirely relevant, leads us not to be too concerned with the calculated cluster centroid's actual value. But instead, we consider it's value related to some augmented feature space.

While it remains that many of these algorithms have an advantage regarding overall pixel classification, a lot of them use at least some type of image averaging filter; it is well known that using averaging filters can cause of the image sharpness to be lost. There is a trade-off to be made between noise robustness and image sharpness, where a poor accuracy at object boundaries can be caused by an imbalanced relationship between these two factors. Often in medical image processing, the loss of some fine-edge data and the information associated with it would be

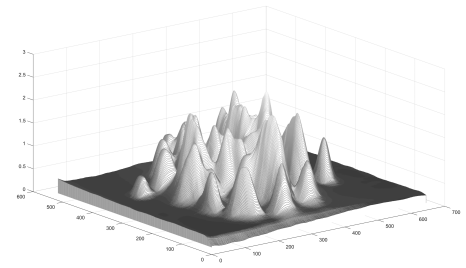

(a) Output of gain term after one iteration

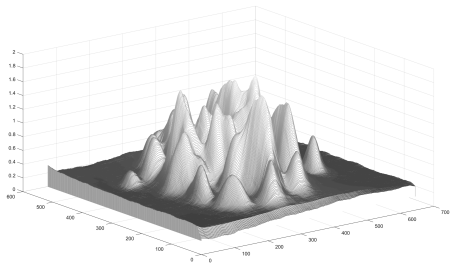

(b) Output of gain term after five iterations

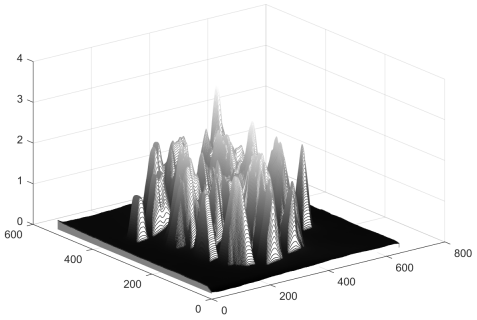

(c) Output of gain term after final iteration

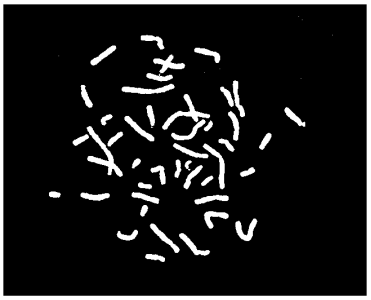

(d) Final output mask of the DAPI chanel

Figure 4.3: Several iterations of the calculated gain field being applied to the DAPI channel

unacceptable. Moreover, the balancing of these factors and their corresponding parameters requires time-consuming manual tuning.

Figure 4.3 shows how the local gain field boosts the pixels with a strong correlation to their neighbours. Additionally, it gives an example of the DAPI channel being segmented using by these methods. Next, the spatial based FCM can then be further extended to map the data-sets feature space into the kernel space.

4.2.3 Kernel methods

An algorithm which has shown a significant level of robustness in numerous fields of pattern recognition is the process of projecting features to higher dimensional spaces using kernel functions. In order to project the clustering results from FCM into a higher dimensional feature space, the FCM algorithm has been extended to use Kernel functions in various research [64, 66, 67, 80]. By projecting any feature

set to an infinitely higher dimensional feature space, it is theoretically possible to ensure there they are linearly separable[64]. However, practically we are not able to project to such a higher dimensional space. Thus, we can instead say that in a practical sense it is probabilistically more likely to find a linearly separable hyperplane within the data by projecting them to a higher dimensional space.

Further development of the FCM algorithm can then see the objective function be projected in higher feature spaces, as shown in eq. (4.5). Using the set of mapping function $\phi = \{\phi_1, \phi_2, \ldots, \phi_M\}$ using $\phi_k(x_i)^T \phi_k(x_j) = K_k(x_i, x_j))$ the kernel function can be defined.

Thus in fuzzy clustering the prototypes of c_k are calculated in the kernel space, therefore, we must update the objective function in eq. (4.2), using the following definition $\phi_k(x_i)^T \phi_k(x_j) = K_k(x_i, x_j)$

$$J = \sum_{i=1}^{N} \sum_{j=1}^{M} \sum_{k=1}^{\Omega} u_{k|i,j}^{q} d\big(\Phi(x_{i,j}), \Phi(c_k)\big)^2 \tag{4.5}$$

When observing the distance function, in eq. (4.5) the $d\big(\Phi(x_{i,j}), \Phi(c_k)\big)^2$ can be simplified easily when using the radial basis function kernel; assuming that we are using the L_2 norm distance metric. This can be demonstrated by expanding this term out to give $K(c_k, c_k) + K(x_{i,j}, x_{i,j}) + 2K(c_k, x_{i,j})$

$$K_{rbf}(\mathbf{x}, \mathbf{x}') = \exp\left(-\frac{||\mathbf{x} - \mathbf{x}'||^2}{2\sigma^2}\right) \tag{4.6}$$

From the Radial Basis Function (RBF) in eq. (4.6) we can easily see that this reduces to $2 - 2K(c_k, x_{i,j})$, vastly simplifying further derivations. For the purpose of this work, let it be assumed that all kernels used will be the RBF kernel.

There exists a large number of kernel functions which could be used, for exam-

ple, a polynomial kernel, there are, however, two primary reasons for choosing the radial basis function. Superficially, it can be selected because finding the derivative to perform Lagrangian optimisation is relatively trivial. This ease of finding the derivative simplifies the algorithm vastly and makes it more flexible for later development. More specifically, the radial basis function is relative to the distance of the desired data-point. To clarify what this means, in essence, it will produce smooth surfaces from lots of data-points. This surface smoothing is ideal when dealing with smoothly varying bias fields as removing it can often cause piece-wise discontinuities within the image, meaning we would have to perform some smoothing as post-processing otherwise. Given these points, it is a good argument for the use of the RBF function as a kernel in this case. Additionally, the RBF function allows for some further parameter tuning. This parameter tuning could be achieved by back-propagation, although in this experiment it was performed empirically. Future work could allow for this level of parameter tuning to be performed; the nature of the image corruptions in the M-FISH image set may mean that the optimisation would need to be performed per-image-set which could be computationally expensive.

4.3 Experimentation: KAFCM segmentation of M-FISH image set.

Using the methods defined in the previous sections the overall framework and corresponding equations will be given in this section. Figure 4.4 shows the overall system design flowchart. First, the DAPI channel is used to create a general pixel mask as this channel binds to all of the chromosomes well. In the mask, the background pixels and non-background pixels are segmented with background pixels denoted as zeros and non-background pixels denoted as ones. This mask is then used to simplify all further segmentation iterations by deleting all of the pixels which are considered as background pixels in the mask in all of the other channel's corresponding pixels. Once again it should be noted that a major issue for M-FISH image segmentation is the large quantity of non-homogeneous regions, these non-homogeneous regions are also exhibited within the inter-chromosome pixels.

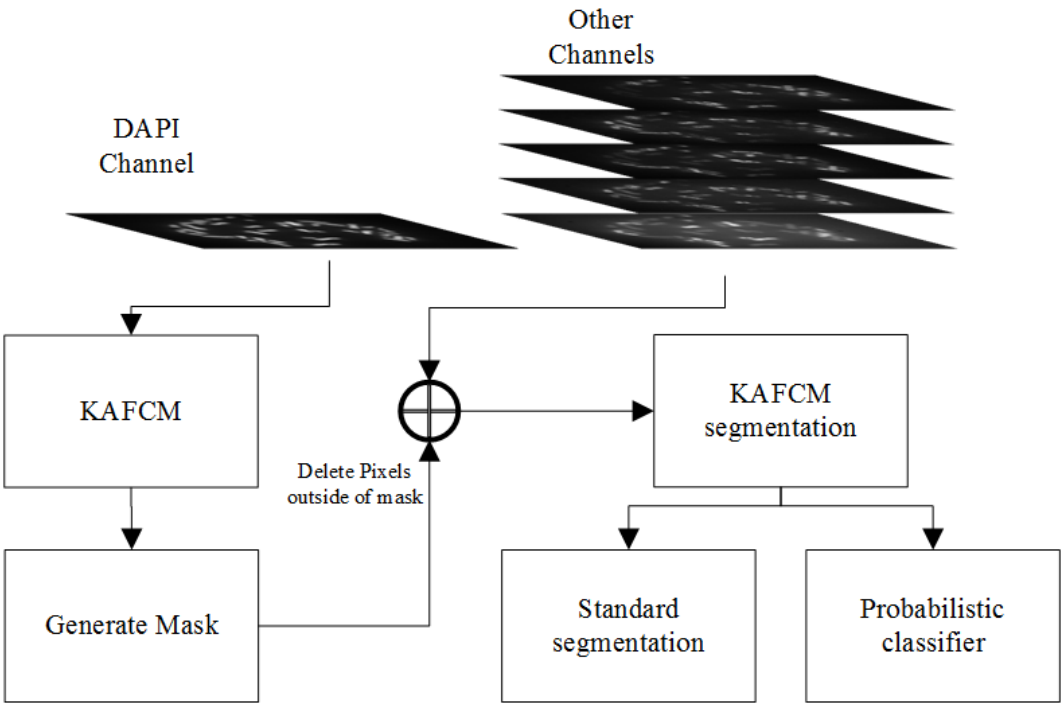

Figure 4.4: Framework of the proposed KAFCM segmentation and probabilistic classifier

4.3.1 The proposed KAFCM algorithm

Equation (4.7) shows this works proposed kernel-based adaptive FCM (KAFCM) segmentation algorithm before being projected to the kernel space, it includes as a constraint a local pixel boosting term η and local pixel intensity averaging function $\Gamma(\eta)$ which is defined in eq. (4.9).

$$\begin{aligned} J = &\sum_{i=1}^{N}\sum_{j=1}^{M}\sum_{k=1}^{\Omega} u_{k|i,j}^{p} \left\| x_{i,j} - \eta_{i,j} c_k \right\|^2 \\ &+ \lambda \sum_{i=1}^{N}\sum_{j=1}^{M} \left(\eta_{i,j} - \Gamma(\eta_{i,j})\right)^2 \end{aligned} \tag{4.7}$$

First, the new kernelised equation needs to be defined, for simplicity we will label the spatial constraint on eq. (4.7), $\eta_{i,j} - \Gamma(\eta_{i,j}) = \eta_{i,j} D_{i \in Z}$. Where Z is an area of pixels surrounding the i^{th} pixel, which is a subset of the whole image. Secondly, we must define the required spatial function Γ. Where H is any Z dimensional matrix, to change the relationship with the spatial constraint. For example H could be a 20×20 normally distributed matrix where Z is a 20×20 pixel area. For the work in this chapter, only an evenly distributed unity matrix was used to ensure we equally considered all of the surrounding pixels.

$$\Gamma(\eta_{i,j}) = \frac{H\eta_i}{(Z_h + Z_v)} \left(\sum_{q \in Z_h} \eta_q + \sum_{r \in Z_v} \eta_r \right) \tag{4.8}$$

$$D_Z = \frac{\sum_{q \in Z_h} \eta_q + \sum_{r \in Z_v} \eta_r}{(Z_h + Zv)} \tag{4.9}$$

Using eq. (4.8) and eq. (4.9) we can reform the objective function as shown in

eq. (4.10).

$$\begin{aligned} J_{KAFCM} = &\sum_{i=1}^{N}\sum_{j=1}^{M}\sum_{k=1}^{\Omega} u_{k|i,j}^{p}\left(1-K(x_{i,j},\eta_{i,j}c_k)\right) \\ &+\lambda\sum_{i=1}^{N}\sum_{j=1}^{M}\left(1-K(\eta_{i,j},\eta_{i,j}D_{i\in Z})\right) \end{aligned} \tag{4.10}$$

To perform Lagrangian optimisation, we first need to derive the partial derivatives with respect to the objective function in eq. (4.10). The result of $\frac{\partial J}{\partial u_{i,j}}, \frac{\partial J}{\partial c_k}, \frac{\partial J}{\partial \eta i,j}, \frac{\partial J}{\partial \lambda i,j}$ are given as follows in eq. (4.11) to eq. (4.14), respectively.

$$u_{k|i,j} = \frac{\left(1-K(x_{i,j},\eta_{i,j}c_k)\right)^{\left(-\frac{2}{p-1}\right)}}{\sum_{l=1}^{\Omega}\left(1-K(x_{i,j},\eta_{i,j}c_l)\right)^{\left(-\frac{2}{p-1}\right)}} \tag{4.11}$$

$$c_k = \frac{\sum_{i=1}^{N}\sum_{j=1}^{M} u_{k|i,j}^{p}\eta_{i,j}x_{i,j}K(x_{i,j},\eta_{i,j}c_k)}{\sum_{k=1}^{\Omega} u_{k|i,j}^{p}\eta_{i,j}K(x_{i,j},\eta_{i,j}c_k)} \tag{4.12}$$

$$\eta_{i,j} = \frac{\sum_{k=1}^{\Omega} u_{k|i,j}^{p}x_{i,j}c_kK(x_{i,j},\eta_{i,j}c_k)}{\sum_{k=1}^{\Omega} u_{k|i,j}^{p}c_kc_kK(x_{i,j},\eta_{i,j}C_k)} \tag{4.13}$$

$$K(\eta_{i,j},\eta_{i,j}D_{i\in Z}) = 1 \tag{4.14}$$

It is important to note that the regularisation term's derivative $\frac{\partial J_\lambda}{\partial \eta_{i,j}}\lambda\sum_{i=1}^{N}\sum_{j=1}^{M}$ $\left(1-K(\eta_{i,j},\eta_{i,j}D_{i\in Z})\right)=0$ can be cancelled out using the result from eq. (4.14). An

additional important observation is that eq. (4.14) is still in the Kernel space, thus we need adapt these equations to factor this into the update algorithm. Considering the inverse Kernel ($K^{-1}(\eta_{i,j}, \eta_{i,j}D_{i\in Z})$) of eq. (4.14) we can easily see that the result of mapping it back to the feature space is $\eta_{i,j} - \eta_{i,j}D_{i\in Z} = 0$, giving the update equation for variable $\eta_{i,j}$ as showin in eq. (4.15).

$$\eta^{+}_{i,j} = \eta_{i,j}D_{i\in Z} \tag{4.15}$$

Having fully derived the optimisation equations we can then go on to describe the algorithmic process, is shown in algorithm 1.

Algorithm 1 Updated FCM algorithm

procedure OPTIMISE PARAMETERS
  Initialise: $\eta_{i,j} = 1 \; \forall \; (i = 1,\ldots,N); (j = 1,\ldots,M)$
  $c_k = rand \; \forall \; (k = 1,\ldots,\Omega)$
  loop:
  $u^{+}_{k|i,j} \leftarrow \frac{\left(1-K(x_{i,j},\eta_{i,j}c_k)\right)^{(-\frac{2}{p-1})}}{\sum_{l=1}^{\Omega}\left(1-K(x_{i,j},\eta_{i,j}c_l)\right)^{(-\frac{2}{p-1})}}$
  $c^{+}_{k} \leftarrow \frac{\sum_{i=1}^{N}\sum_{j=1}^{M} u^{p}_{k|i,j}\eta_{i,j}x_{i,j}K(x_{i,j},\eta_{i,j}c_k)}{\sum_{k=1}^{\Omega} u^{p}_{k|i,j}\eta_{i,j}K(x_{i,j},\eta_{i,j}c_k)}$
  $\eta_{i,j} = \frac{\sum_{k=1}^{\Omega} u^{p}_{k|i,j}x_{i,j}c_kK(x_{i,j},\eta_{i,j}c_k)}{\sum_{k=1}^{\Omega} u^{p}_{k|i,j}c_kc_kK(x_{i,j},\eta_{i,j}C_k)}$
  $\eta^{+}_{i,j} \leftarrow \eta_{i,j}D_{i\in Z}$
  if $max(u^{+}_{ik} - u_{ik}) < \varepsilon$ **then**
    break;
  else
    goto *loop*.
  end if
end procedure

4.3.2 Proposed Classification Algorithm

Performing segmentation and classification on M-FISH images can often encounter images which can be labelled as 'hard to karyotype'. These hard to karyotype images are the images that the segmentation algorithm performs very poorly and results in a very bad classification rate. In this chapter, the focus is on how to improve the classification rates on these 'hard to karyotype' images by changing the defuzzification method. Firstly, it should be noted that the classification is not just over one image, but six images or "channels", each channel having independent intensity distributions. Secondly, as can be observed from the results of the segmentation, although a pixel may be incorrectly segmented on one channel, the corresponding pixel on another channel may still have a relatively higher level of certainty. So the matrix of all channels would be: $\mathbf{x} = [x_{i,j}^{(1)}, x_{i,j}^{(2)}, x_{i,j}^{(3)}, x_{i,j}^{(4)}, x_{i,j}^{(5)}]$ where $x_{i,j}^{(c)} \in 0,1, i = 1,2,\ldots,N, j = 1,2,\ldots,M, c = 1,\ldots,m$. Here, N and M are the dimensions of the image and m is the number of channels.

The defuzzification a fuzzy clustering algorithm when performing image segmentation normally takes a winner takes all approach. However, in the proposed algorithm we approach it from a more probabilistic perspective. Using output of the KAFCM algorithm we can create probabilistic classifier by using the matrix of responsibilities of each channel $U = [\ \vec{u}_1\ \vec{u}_2, \vec{u}_\alpha, \ldots\ , \vec{u}_m\ ]^T$ where each $\vec{u}$ is a vector of the responsibilities derived from the KAFCM for each of the image channels such that $\vec{u}_\alpha = [u_1, u_2, u_i, \ldots, u_D]$, $i \in D$. Where D is the whole pixel area of the image converted to a vector; The matrix U is a $D \times m$ dimensional matrix. Thus we can consider each of the responsibilities the level of certainty that the KAFCM algorithm had that the corresponding pixel belonged to the chromosome class.

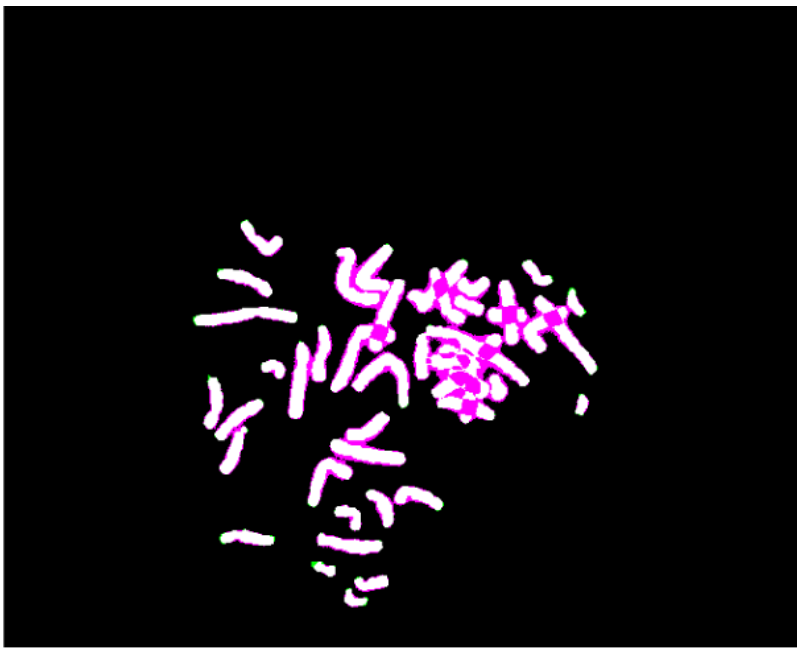

(a) Segmentation result from DAPI channel

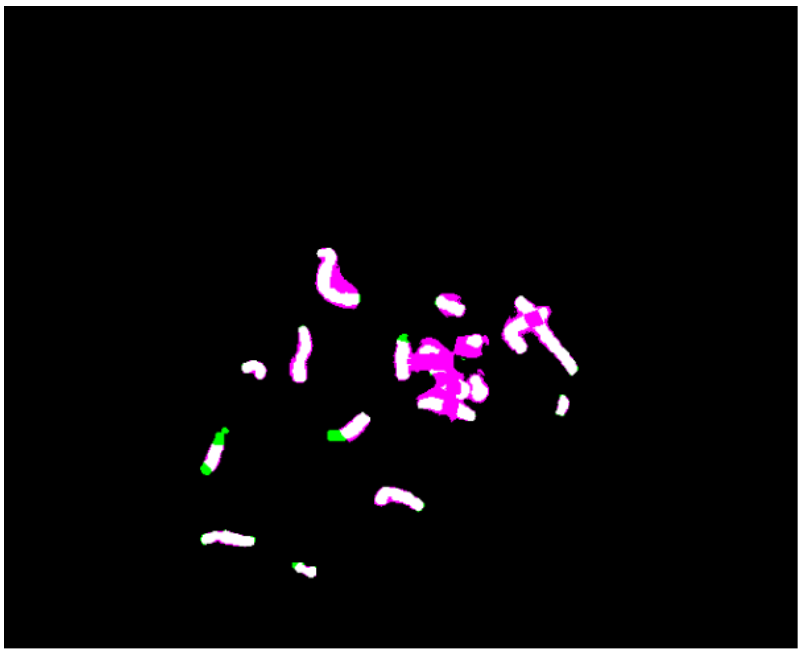

(b) Segmentation result from AQUA channel

Figure 4.5: Example results from a hard to cluster image, where pink represents either a background pixel being segmented as a chromosome pixel or an overlap of chromosome pixels. And green a chromosome pixel segmented as a background pixel

$$
\begin{aligned}
p(C_n|U_i) &= \frac{p(C_n)\ p(U_i|C_n)}{p(U_i)} \\
\hat{y} &= \underset{n\in\{1,\ldots,m\}}{\operatorname{argmax}}\ p(C_n)\prod_{i=1}^{n} p(U_i|C_n)
\end{aligned}
\tag{4.16}
$$

From this, and the assumption of conditional Independence, we implemented the well-known Naive Bayes classifier shown in eq. (4.16) using the six channels responsibilities matrix U_i as input for each pixel into the classifier, shown in eq. (4.19).

First, we have to form a matrix of likelihoods for each pixel of each channel. We define the vector for pixel i as $u_i = [u_i^{(1)}, u_i^{(2)}, u_i^{(\alpha)}, \ldots, u_i^{(m)}]^T$ where m is the number of channels in the image. Furthermore, we define each vector of likelihoods of each channel based on the distance measurement from eq. (4.10); For simplification, we omit the subtraction term given in eq. (4.17). Where the α indices indicate which channel they belong to.

$$
u_i^{(\alpha)} = \frac{K(x_i^{(\alpha)}, \eta_i^{(\alpha)} c_k^{(\alpha)})}{\sum_{l=1}^{\Omega}\left(K(x_i^{(\alpha)}, \eta_i^{(\alpha)} c_l^{(\alpha)})\right)}
\tag{4.17}
$$

Before further discussion there are two observations to make. Firstly, we are only interested in the likelihood that this pixel belongs to the chromosome class, and secondly that sum of the likelihoods for each pixel is equal to one. Which can be represented using $\sum_{k=1}^{\Omega} \frac{K(x_{i,j}^{(\alpha)}, \eta_{i,j}^{(\alpha)} c_k^{(\alpha)})}{\sum_{l=1}^{\Omega}\left(K(x_{i,j}^{(\alpha)}, \eta_{i,j}^{(\alpha)} c_l^{(\alpha)})\right)} = 1$.

$$U_i = \begin{bmatrix} u_i^{(1)} & u_i^{(2)} & u_i^{(\alpha)} & \cdots & u_i^{(m)} \\ u_i^{(1)} & \ddots & & & \vdots \\ u_i^{(1)} & & u_i^{(\alpha)} & & \vdots \\ \vdots & & & \ddots & \vdots \\ u_i^{(1)} & \cdots & \cdots & \cdots & u_i^{(m)} \end{bmatrix}$$
$$C = \begin{bmatrix} c_1^{(1)} & c_1^{(2)} & c_1^{(\alpha)} & \cdots & c_1^{(m)} \\ c_2^{(1)} & \ddots & & & \vdots \\ c_\beta^{(1)} & & c_\beta^{(\alpha)} & & \vdots \\ \vdots & & & \ddots & \vdots \\ c_n^{(1)} & \cdots & \cdots & \cdots & c_n^{(m)} \end{bmatrix} \tag{4.18}$$

The classifier can then be created by forming the matrix U_i and a matrix c_β of all the possibilities from the previously mentioned combinatorial labelling scheme into a single matrix such that $C = [c_\beta^1, c_\beta^2, c_\beta^\alpha, \ldots, c_\beta^m]$, where m is the number of classes; for example $c_1 = [1\ 0\ 0\ 1\ 0\ 0]$. Finally we form two augmented matrices U and C so that each row of matrix C is c_β and each column of matrix U is $u^{(\alpha)}$. To classify each pixel we use the kernel form of the absolute difference between U and C chose the class for each pixel based on the output of eq. (4.19), remembering the earlier simplification of on eq. (4.17). The result of of $K(C, U_i)$ in eq. (4.19) is an m element vector, thus the output of the classifier $\hat{y}_i$ is the element of the vector with the highest value.

$$\hat{y}_i = \underset{\beta \in \{1,\ldots,n\}}{\operatorname{argmax}} \sum_{\alpha=1}^{m} K(C, U_i) \tag{4.19}$$

4.3.3 Experimental setup

In this chapter the algorithm was tested on 342 images over 57 sets of Karyotyped cells, these are from a public dataset[81–83] containing hand-segmented M-FISH images from Advanced Digital Imaging Research which is now maintained and available from the Laboratory for Image & Video Engineering via. http://live.ece.utexas.edu/research/mfish.html. Unlike comparative studies in the results, to prove the potential of the proposed algorithm we compared our classifiers performance on problematic images within the dataset, this also includes images with many overlaps. Each iteration of proposed algorithm took approximately 51s using a quad-core i7-4870HQ CPU at 2.50GHz and 16GB of RAM. The following sections will present the results with an analysis followed by concluding remarks.

4.4 Results

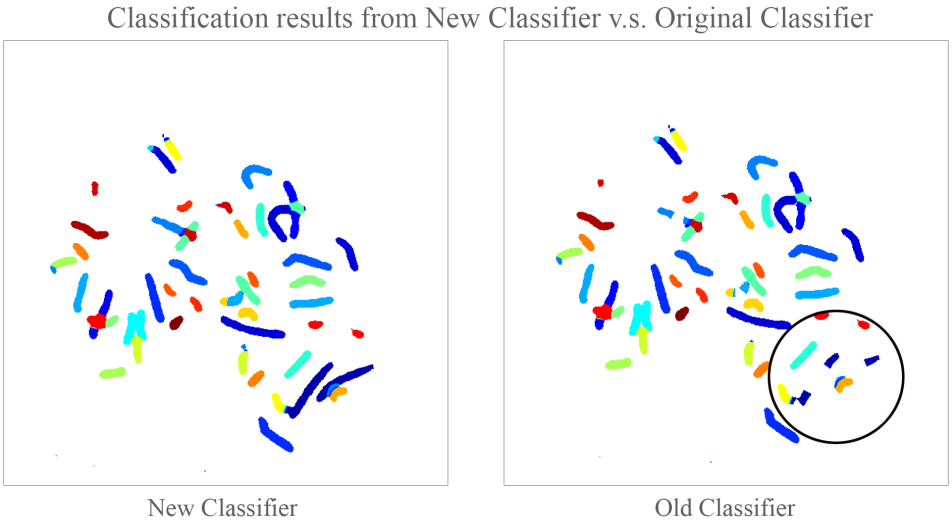

Figure 4.6: Comparison of the output from both classifiers.

4.4.1 Segmentation results

The results show the classification results for chromosomes classified by the KAFCM with probabilistic classifier compared to the ground truths provided in

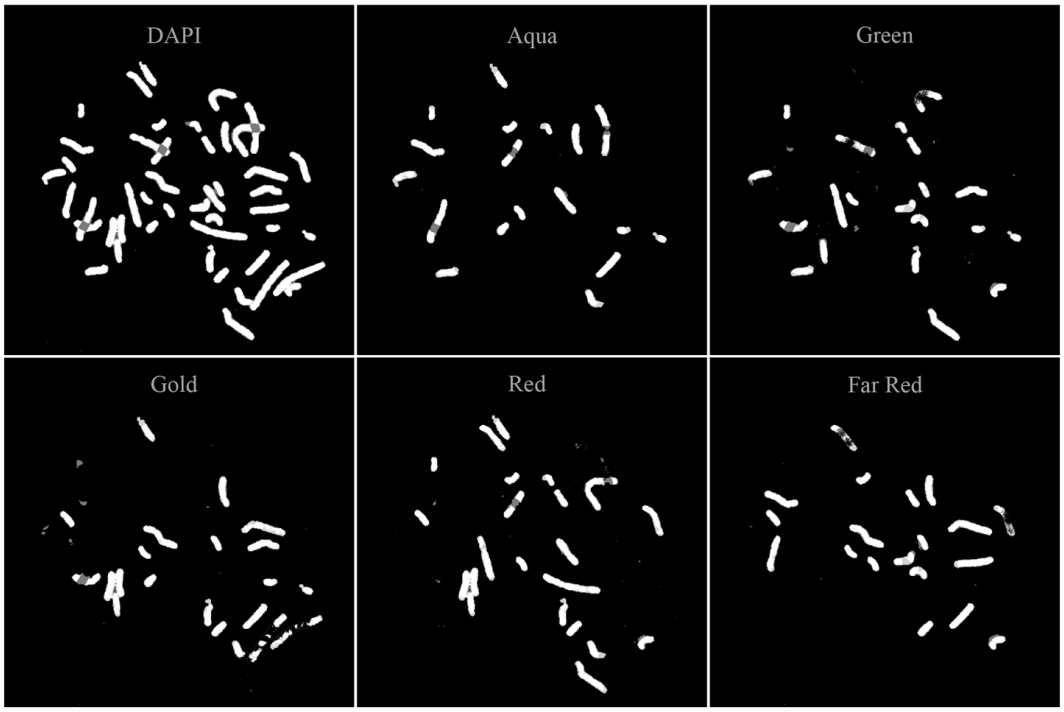

Figure 4.7: Segmentation results for each channel

the dataset, and the overall CR and FR for algorithm. The CR and FR are derived from the combinatorial logic for M-FISH karyotyping[84]. In short, this states that, based on the logic table, if a pixel from a particular image channel is required for classification to be segmented as a chromosome pixel, then for that channel it is considered as a correct segmentation. Conversely, it will be considered to be a false positive if it has been incorrectly segmented as a background pixel. For every set of results, a comparative result from other methods is given. It can be seen that the proposed method has shown an overall better performance when compared using the hard to Karyotype images. However, the running time is restrictively long for implementation into a real clinical setting. Importantly, there was no pre-processing or post-processing of the images in this Chapter, potentially the results have been adversely affected due to the effects of some background noise as this is observable as being incorrectly segmented in most images. Table 4.2 shows the results for the classification of each chromosome, and table 4.3 shows the CR and FR from the

Table 4.1: Accuracy per chromosome (%) of both implemented classifiers and their difference using subset of data

Chromosome Number	Number of Pixels Correctly classified (%)		
	Standard Classifier	Proposed Clasifier	Difference
1	62.9	79.4	16.5
2	66.7	87.9	21.2
3	86.5	90.9	4.4
4	52.2	80.0	27.8
5	74.6	77.9	3.2
6	77.4	84.7	7.3
7	75.8	89.9	14.2
8	64.8	75.8	11.0
9	62.9	78.0	15.1
10	65.2	92.4	27.2
11	67.3	86.1	18.8
12	81.5	84.3	2.9
13	55.2	66.1	11.0
14	53.9	77.0	23.1
15	44.0	66.9	23.0
16	68.1	74.8	6.8
17	80.2	90.8	10.5
18	61.7	82.3	20.6
19	67.4	84.6	17.2
20	72.4	90.3	17.9
Average	67.0	82.0	15.0
s.t.d	10.7	7.6	7.7

proposed method. From the experimental results, it can be seen that the proposed method demonstrates comparable if not better results, with a CR of 87.2% and FR of 2.63%, this result could be improved by some further development of the spatial constraint as well as some pre-processing of the images.

4.4.2 Comparison of classifiers

For the easy to segment images in the datasets, there was little improvement shown when using the proposed classifier. Therefore, in this Chapter the poorly performing images were separated and used to create a new subset of images for comparison;

Table 4.2: Comparison of accuracies per chromosome (%) with proposed algorithm

	Number of Pixels Correctly classified (%)		
Chromosome Number	KAFCM	IAFCM	FCM
1	79.4	95.5	78.2
2	87.9	91.5	82.1
3	90.9	97.0	75.2
4	80.0	85.9	84.6
5	77.9	96.7	74.6
6	84.7	84.2	85.2
7	89.9	82.7	89.2
8	75.8	93.1	75.0
9	78.0	93.1	77.0
10	92.4	90.4	92.0
11	86.1	89.4	85.9
12	84.3	93.2	83.3
13	66.1	87.2	65.3
14	77.0	83.1	76.2
15	66.9	85.9	66.4
16	74.8	79.4	74.5
17	90.8	80.4	90.4
18	82.3	91.7	81.8
19	84.6	81.7	84.2
20	90.3	87.9	89.6
Average	82.0	88.5	80.5
s.t.d	7.6	5.5	7.5

Table 4.3: Comparative results for both CR and FR

Comparison of reported CR and FR ratios with proposed algorithm			
	Accuracy rates (%)		
	KAFCM	IAFCM	FCM
CR	87.20	89.5	92
FR	2.63	3.6	9.7

A detailed description of the dataset can be found in chapter 3. The ”new subset” of images was created by selecting images which showed any chromosome group being misclassified below 70%. The reason for creating a subset of images was to highlight the potential differences between the two proposed methods. Using

only the new subset we analysed the results from each classifier, as can be seen in table 4.1, the new classifier showed an increase in performance for nearly all of the chromosome classes. Figure 4.6, shows some good examples of how the proposed classifier manages to label some of the chromosomes pixels correctly which were otherwise completely lost in the original method. Originally, the pixels were lost due to the noise and inhomogeneities contained in at least one of image channels; thus causing the segmentation algorithm to improperly segment the pixels. However, because we considered the probabilities across all of the image channels we were able to reclassify the pixels correctly. From these results, the classifier shows a great deal of promise, with a maximum improvement of 27.8% on the classification of chromosome four and an overall improvement of 15% across all chromosomes; this improvement was achieved without changing the segmentation algorithm in any way. This improvement of the results shows that improvement in classification rate can be achieved by considering the membership functions across all of the image channels rather than just the segmentation results. In comparison to other works, the proposed system performed within a relatively similar accuracy, with a CR of 82.2% and FR of 2.63%. All of the experiments were performed using a unity matrix for the spatial biasing term H in eq. (4.9) and we found that a size of 10×10 pixels performed best.

4.5 Discussion

This chapter presented an FCM based-algorithm, the segmentation acurracy of which has been improved by modifying it to consider local spatial data and then projected into the kernel space. Additionally, a probabilistic defuzzification method based on the membership functions of the segmentation results was developed to further improve the classification accuracy of the proposed KAFCM algorithm.

While the results of the proposed algorithm contained comparatively similar results to other methods, it did show a significant improvement on images which were otherwise difficult to classify; the difficulty was in part, due to increased noise or artefacts introduced during the imaging process or high amounts of overlapping chromosomes. The proposed classifier did show some improvements in the classification accuracy of these images. However, some inter-chromosome misclassifications were also shown; due to the fact that they tend to appear inside a large group of correctly classified pixels it is possible this could be corrected post-classification. Overall, the classifier does show a great deal of potential, with a maximum improvement of 27.8% on the classification of chromosome four and an overall improvement of 6.5% across all chromosomes, all achieved without altering the segmentation algorithm. This improvement in results shows that by considering the membership functions across all of the channels rather than just the hard segmentation results, it is possible to improve the overall classification. Importantly for some chromosome sets, it exhibited around 95% classification rate for most chromosomes in the set. However, this only occurs in very ”well-behaved” image sets.

Observing the results in table 4.2, the classification accuracy of the IAFCM algorithm is higher for most chromosomes. This higher accuracy is because these are the published results from their journal paper for which we cannot obtain the dataset. Furthermore, they state that they only used ten images which we can assume were specially selected because of their high performance. Thus, it is incredibly difficult to compare the performances of these two methods. However, we believe that considering the extremely close accuracy levels within 6% when using an image subset of difficult to segment images, the results are valid and at least comparable.

Finally, it can be seen that the proposed system is useful for this specific ap-

plication. However, it remains a potential interest to see how well the proposed probabilistic classifier can work on other datasets. Thus to improve this aspect of the classifier, further research is needed. Additionally, further investigations on the algortihms performance on other datasets need to be carried out. In future work, an investigation on how changing the spatial term H in eq. (4.8) will affect the results. In the next Chapter, to further develop the algorithm, the performance on some synthetic image data and a real-world image will be performed.

Chapter 5

Method 2: Local-region clustering informed level-set methods

5.1 Overview

This method is a development of the previous chapter, utilising a hybrid method of both fuzzy clustering and level sets. A description of the related methods will be given and then an explanation of the system methodology.

To properly develop a hybrid method, it is important to understand the basic background of the active-contour model, and the various types of models which are being used today in research. The basic idea of the active-contour is that of contour evolution, where a force or flow is optimised until it can find an object's boundary. The method implemented to achieve this change based on the data being used to evolve its progress. As such, it is useful to know the normal types of active-contour models, which are, global region-based[85–88], edge-based[89, 90], hybrid edge-region methods[91, 92], local[93–96] and local-global region based models[97, 98].

Many problems in medical imaging such as tumours can be modelled as deformable objects [92, 99, 100] and certainly when trying to solve the issue of image registration there has been much success with when using the deformable model.

These deformable models are successful by using edge detection and registering the local elements of the images[101]. In general, the edge-based methods are achieved by growing a level-set on the pixels to find the tumour boundaries; Using a gradient stop function they can successfully locate a continuous boundary, they are however sensitive to noise within images and unable to handle weak gradient boundaries. From this, we can look into region-based models as they tend to have a better performance on objects with weak gradient boundaries.

5.2 Methodology

5.2.1 Fuzzy clustering

The Fuzzy clustering method used in this investigation was built upon from previous work found in Dougherty and You using a kernel-based adaptive fuzzy C-means (KAFCM) algorithm, for brevity we will not discuss it thoroughly in this chapter, but will at least give some of the corresponding eqs. (4.9) to (4.11)

Equation (4.10) in chapter 4 on page 37 is the primary focus for the objective function of the FCM step in fig. 5.1. The advantages of the KAFCM algorithm are that it is very good at segmenting images with unclear gradient boundaries and at filtering out pixel intensity inhomogeneities. However, it has trouble with smoothly varying gradient boundaries. As this algorithm is not the main topic of the discussion, the reader is directed to Chapter 4, section 4.3.1 for more information.

5.2.2 Level sets

As shown in He et al., Chunming Li et al. a level set can be defined as the evolution of a curve based on the force in the normal direction. If we consider the surface as a function phi and we call the current surface the c-set, we can define it as shown in eq. (5.1). However, we are interested in the surface which exactly matches our

target shape, which we define as the point where $c = 0$. If we parameterise the previous equation with t and look at the point where it is equal to 0, then it will become eq. (5.2); this can be further simplified into eq. (5.3) using more compact notation and noticing that the left-hand side is the gradient.

$$\phi(x) = 0 \tag{5.1}$$

$$\frac{\partial \phi}{\partial x(t)} \frac{\partial x(t)}{\partial t} + \frac{\partial \phi}{\partial t} = 0 \tag{5.2}$$

$$\nabla \phi(X)_t + \phi_t = 0 \tag{5.3}$$

As the evolution of the curve is in the normal, that is the force F. we can replace X_t to make eq. (5.4). Finally yielding the level-set equation as eq. (5.5) for the surface evolution speed.

$$\begin{aligned} \nabla \mathbf{F} \frac{\nabla \phi}{\|\nabla \phi\|} + \phi_t(X_t) + \phi_t = 0 \\ \mathbf{F}\|\nabla \phi\| + \phi_t(X)_t + \phi_t = 0 \end{aligned} \tag{5.4}$$

$$\phi_t = -\mathbf{F}\|\nabla \phi\| \tag{5.5}$$

Finally using the finite difference method and theories behind gradient decent, we can obtain the update function in eq. (5.6) which will be used in the level set part of the system flow diagram in fig. 5.1 on page 54.

This hybrid method of using both the fuzzy-clustering methods and level set methods is labelled as a Local-region clustering informed level-set (LRCLS) method.

$$\phi' = \phi + \nabla t \mathbf{F} \|\nabla \phi\| \tag{5.6}$$

5.3 Experimentation: LRCLS segmentation of the synthetic image set

5.3.1 Proposed hybrid algorithm

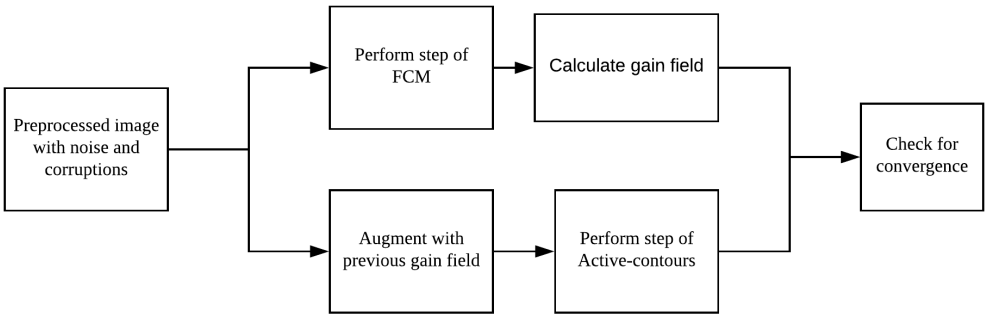

Figure 5.1: System flow diagram of a Local-region clustering informed level-set method

The novelty of this method is how it fuses the standard FCM with gain field calculation with the active contours algorithm. By using the gain-field calculations we are able to change the way that the active contours method evolves the curve to find the object boundaries by reducing the effects of a smoothly varying gradient across the image.

5.3.2 Experimental setup

For this experiment, we used a selection of both real and synthetic images, fig. 5.2 shows all of the original images used. Images A, C and D are all synthetic images which had a bias field added to them; Image B is also a well known synthetic image which has been used in numerous other studies; and Image E is a real world image taken from a karyotype. For each experiment the same parameters were used for each method, and each method used the same image as the input.

The reasons to use a synthetic dataset are various. Initially, we first need to acknowledge that the real-world image dataset used is limited in the number of

images, especially once they have been formed into a new subset as described on page 46. While these synthetic images may be relatively different to the M-FISH image dataset, they do however share some similar intrinsic properties which make them suitable for testing the new algorithm with more images than is available with the real-world dataset.. Additionally, the artificial bias and additive noise shows a similar response in terms of accuracy results as those shown in the real-world image dataset. This method of creating synthetic images allows to testing new algorithm within a controllable environment, such that, we can try to figure out in a controlled way which parts of the algorithm are not working well.

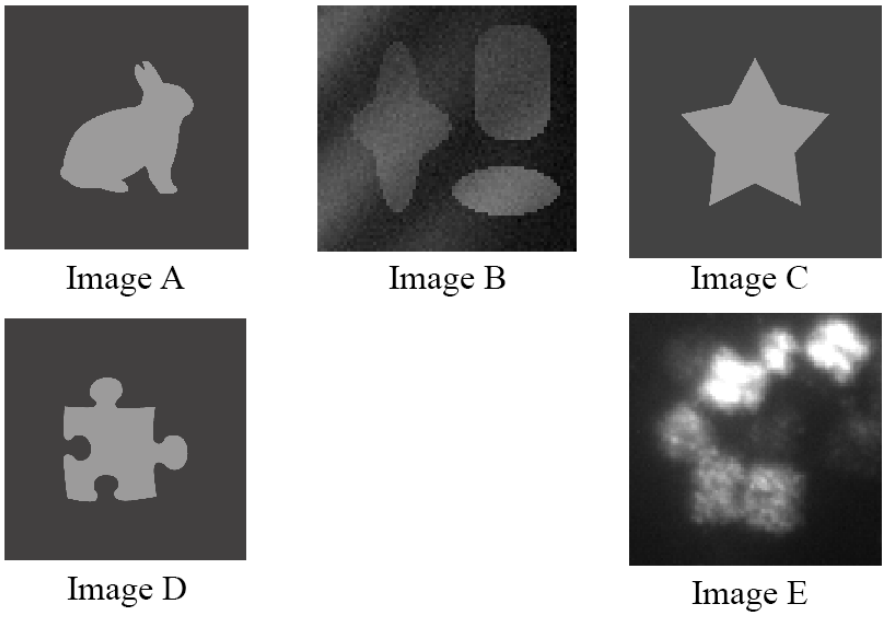

Figure 5.2: Original Images used in Chapter 2 study.

5.4 Results

In the below figures, presented are some example images and the results of the investigated method along with comparisons to other methods. For all of the figures, the following is true for their labelling:

1. The original image
2. Local Statistical Level Set Method with Intensity Inhomogeneity
3. Standard FCM algorithm
4. KAFCM algorithm
5. Standard level-set method
6. The proposed method

The figs. 5.3 and 5.5 to 5.7 are all using synthetic images self-generated for the purpose of these experiments, whereas fig. 5.4 is using a well-known synthetic image used in much literature and fig. 5.8 is using a real medical image. In most cases the investigated method performs quite similarly with the previous work on a kernel based FCM algorithm; but once high levels of noise are introduced, as seen in fig. 5.3, the proposed method vastly outperforms the previous methods. Similarly, in fig. 5.4, the method outperforms all other methods on the well-known synthetic image. For the last image of the real medical image, it also outperforms the other methods quite well.

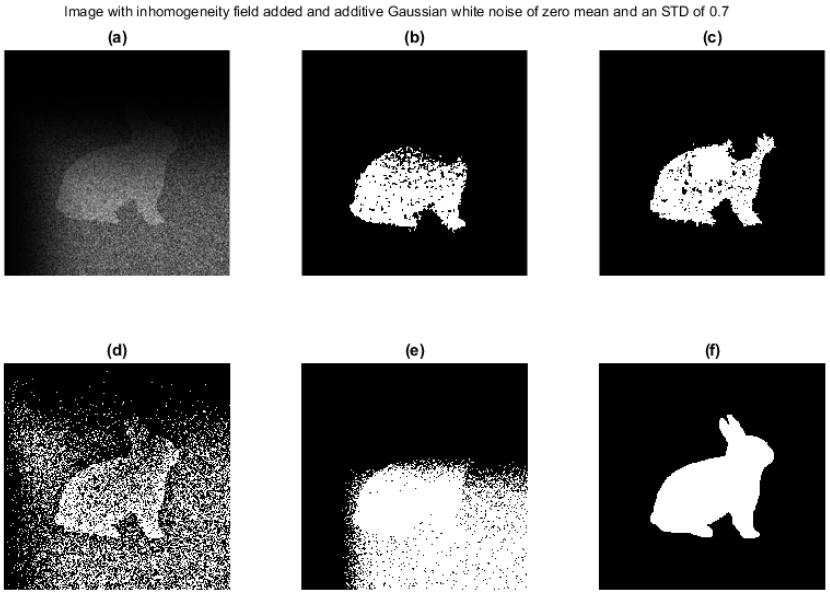

Figure 5.3: Showing results on Image A1 (rabbit-shaped synthetic image) and high levels of noise

Table 5.1: Showing results on Image A1 (rabbit-shaped synthetic image) and high levels of noise

Image A1 with additive Guassuan noise, zero mean, STD 0.7

Method	CR (%)	FR (%)	Precision	Recall	F-score
LS-level set	62.99	1.89	86.43	62.99	72.87
FCM	75.54	0.53	96.45	75.54	84.73
KAFCM	59.79	24.40	31.86	59.79	41.57
Level-set	75.39	30.93	31.75	75.39	44.68
Proposed	97.94	0.77	96.05	97.94	96.99

Table 5.2 and fig. 5.4 show the results using Image B. From this we can see that proposed method works much better than both the KAFCM and the level set method, most likely this is due to the added gradient and the unusual topology, working against the weakness of both methods.

Table 5.3 and fig. 5.5 show the results using Image C. From this we can see that both the KAFCM and the proposed method work equally well, most likely this is due to the added gradient not crossing any curved borders and the shape having

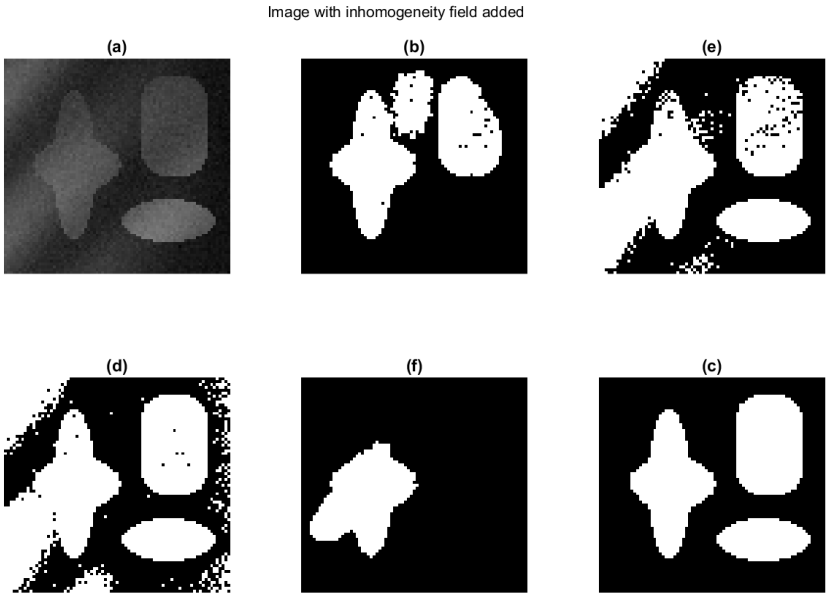

Figure 5.4: Showing results on Image B (a well known set of synthetic image)

Table 5.2: Showing results on Image B (a well known set of synthetic image)

Image B from a well known set of synthetic images

Method	CR (%)	FR (%)	Precision	Recall	F-score
LS-level set	71.32	6.78	83.40	71.84	77.19
FCM	94.36	22.26	66.93	94.99	78.53
KAFCM	98.12	27.07	63.36	98.68	77.17
Level-set	33.27	4.81	76.68	33.37	46.50
Proposed	98.11	0.44	99.06	98.74	98.90

well defined edges.

Here in fig. 5.5 it can be observed that while it can counteract the short-falls of a standard level-set algorithm, the performance is basically identical to the KAFCM algorithm showing. The same can be seen in fig. 5.6, where a low level of noise does not impact the performance of the KAFCM element of the algorithm.

The most interesting result is shown in fig. 5.8, as can be observed, and as would be expected, the level-set method outperforms the KAFCM algorithm. This is due to the smooth boundaries and multi-topological nature of the image. It is also

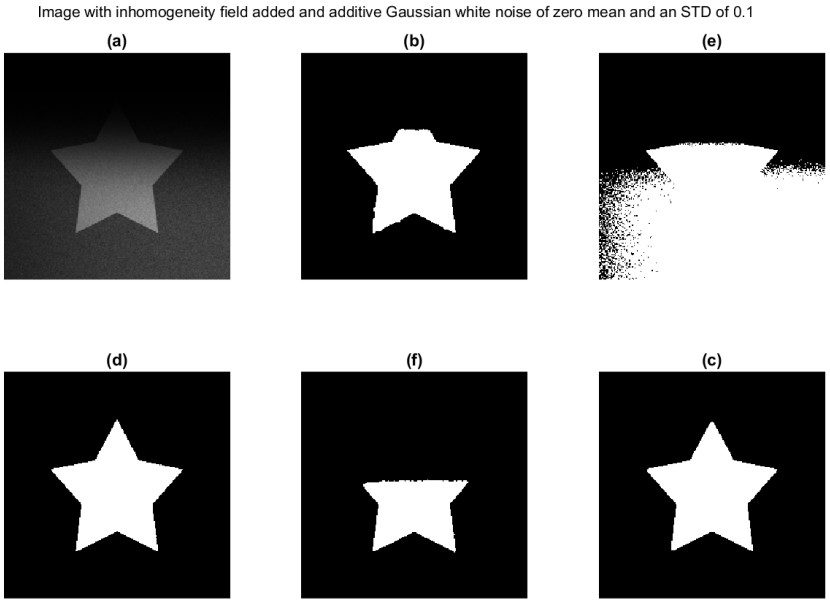

Figure 5.5: Showing results on Image C (star-shaped synthetic image)

Table 5.3: Showing results on Image C (star-shaped synthetic image)

Image C with additive Guassuan noise, zero mean, STD 0.1

Method	CR (%)	FR (%)	Precision	Recall	F-score
LS-level set	94.06	0.55	0.97	0.94	0.95
FCM	86.80	43.68	0.27	0.87	0.41
KAFCM	99.55	0.22	0.99	1.00	0.99
Level-set	61.00	0.24	0.98	0.61	0.75
Proposed	99.54	0.23	0.99	1.00	0.99

observed that the level-set method is immune to the discontinuous regions within the object boundaries. However, the KAFCM algorithm was able to ignore the fuzzy boundaries caused by the intensity inhomogeneities and correctly segment the regions at the top of the image. The most important observable fact is that the new method is able to combine both of these methods to ultimately outperform them both.

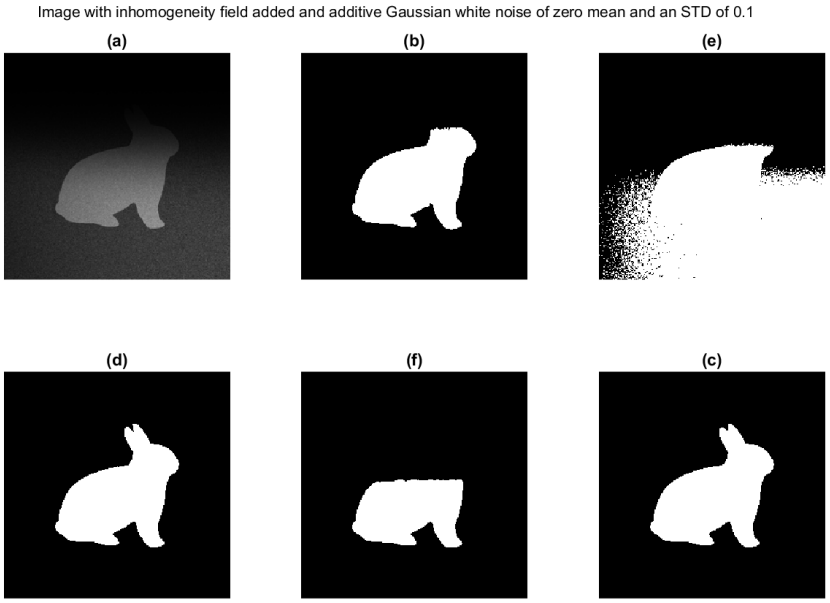

Figure 5.6: Showing results on Image A (rabbit-shaped) synthetic image

Table 5.4 and fig. 5.6 show the results using Image A. From this we can see that both the KAFCM and the proposed method work equally well, most likely this is due to the added gradient not crossing any curved borders and the shape having well defined edges.

Table 5.4: Showing results on Image A (rabbit-shaped) synthetic image

Image A with additive Guassuan noise, zero mean, STD 0.1

Method	CR (%)	FR (%)	Precision	Recall	F-score
LS-level set	94.29	0.45	97.58	94.37	95.94
FCM	85.44	37.42	30.36	85.59	44.82
KAFCM	99.47	0.19	99.02	99.53	99.27
Level-set	71.24	0.26	98.12	71.36	82.63
Proposed	99.28	0.12	99.36	99.32	99.34

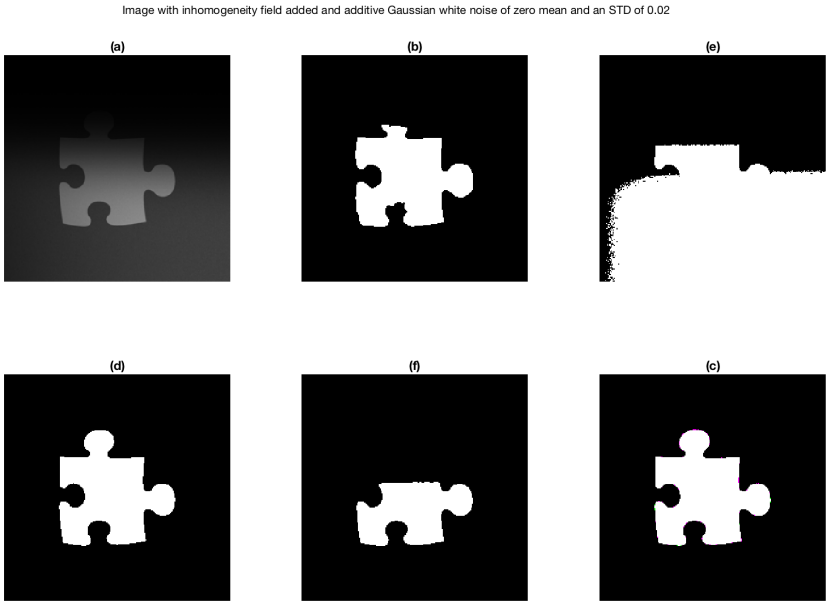

Figure 5.7: Showing results on Image D (jigsaw-shaped synthetic image)

5.5 Discussion

This Chapter presented a hybrid algorithm based on KAFCM and Level-sets equations to perform segmentation on synthetic images. The proposed method was compared with four other methods, and for each set of experiments, the proposed performed either similarly or had a much superior performance. Given the much higher performance of this hybrid method on the synthetic images, a natural progression would be to begin testing on the original real-world dataset. However, first, a more

Table 5.5: Showing results on Image D (jigsaw-shaped synthetic image)

Image D with additive Guassuan noise, zero mean, STD 0.1

Method	True Positive (%)	False Positive (%)	Precision	Recall	F-score
LS-level set	94.59	0.66	96.31	94.59	95.45
FCM	83.98	42.90	26.16	83.98	39.90
KAFCM	98.62	0.09	99.49	98.62	99.05
Level-set	63.15	0.13	98.86	63.15	77.07
Proposed	98.79	0.11	99.40	98.79	99.09

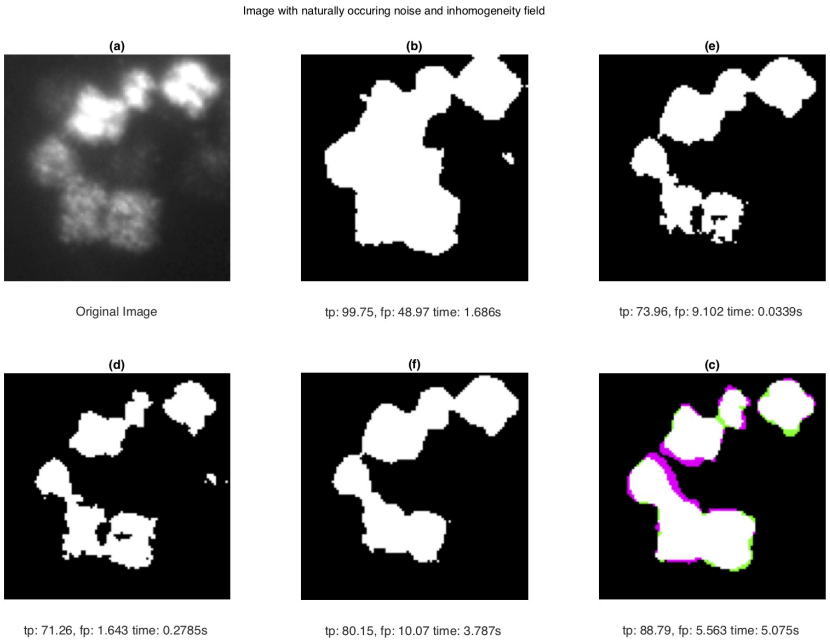

Figure 5.8: Showing results on Image E (real-world karyotype image)

Table 5.6: Showing results on Image E (real-world karyotype image)

Image E, real karyotype image

Method	True Positive (%)	False Positive (%)	Precision	Recall	F-score
LS-level set	99.30	13.97	70.57	99.30	82.50
FCM	66.98	2.08	91.57	66.98	77.36
KAFCM	61.81	0.92	95.77	61.81	75.13
Level-set	75.49	2.29	91.75	75.49	82.83
Proposed	81.91	0.03	99.91	81.91	90.02

robustly described method should be developed as it already has shown at least anecdotally that this method will out-perform the original KAFCM algorithm. As this hybrid method would still require very time-consuming parameter tuning which may be able to be removed in the updated method, we decided to skip the testing on the real-world dataset and focus on the new method. In terms of results, if we observe table 5.6, we can see that the CR of the proposed method is higher than all other methods in general except for the standard level-set. However, the standard

level-set has a very high FR. Overall, we should expect the best method to have the highest F-score as this is the ratio of the false positive to true positive both of which have a correlation to FR and CR. The proposed method has the best F-score for all of the experiments.

Chapter 6

Method 3: Fuzzy region based level set

6.1 Overview

When beginning this investigation, it can be noted that one of the biggest issues facing pixel based segmentation methods such as those based on FCM are when the target image contains highly non-homogeneous such as the image found in fig. 6.2 and the results in table 6.1. From this it can be seen that both a Distance Regularized Level Set Evolution (DR-level set)[105] and the basic FCM algorithm perform relatively poorly. Even the previous methods used in the study do not perform too well, while the newest method in this chapter shows a marked improvement.

Table 6.1: Showing results on MRI image for all investigated methods

Image 3Tb

Method	CR (%)	FR (%)	Precision	Recall	F-score	Specificity
DR-level set	68.18	5.67	80.84	68.20	73.98	94.33
FCM	99.71	26.49	56.90	99.78	72.48	73.51
KAFCM	87.64	2.80	91.66	87.69	89.63	97.20
LRC Level-set	89.42	2.89	91.57	89.61	90.58	97.10
Proposed	89.37	1.63	95.06	89.43	92.16	98.37

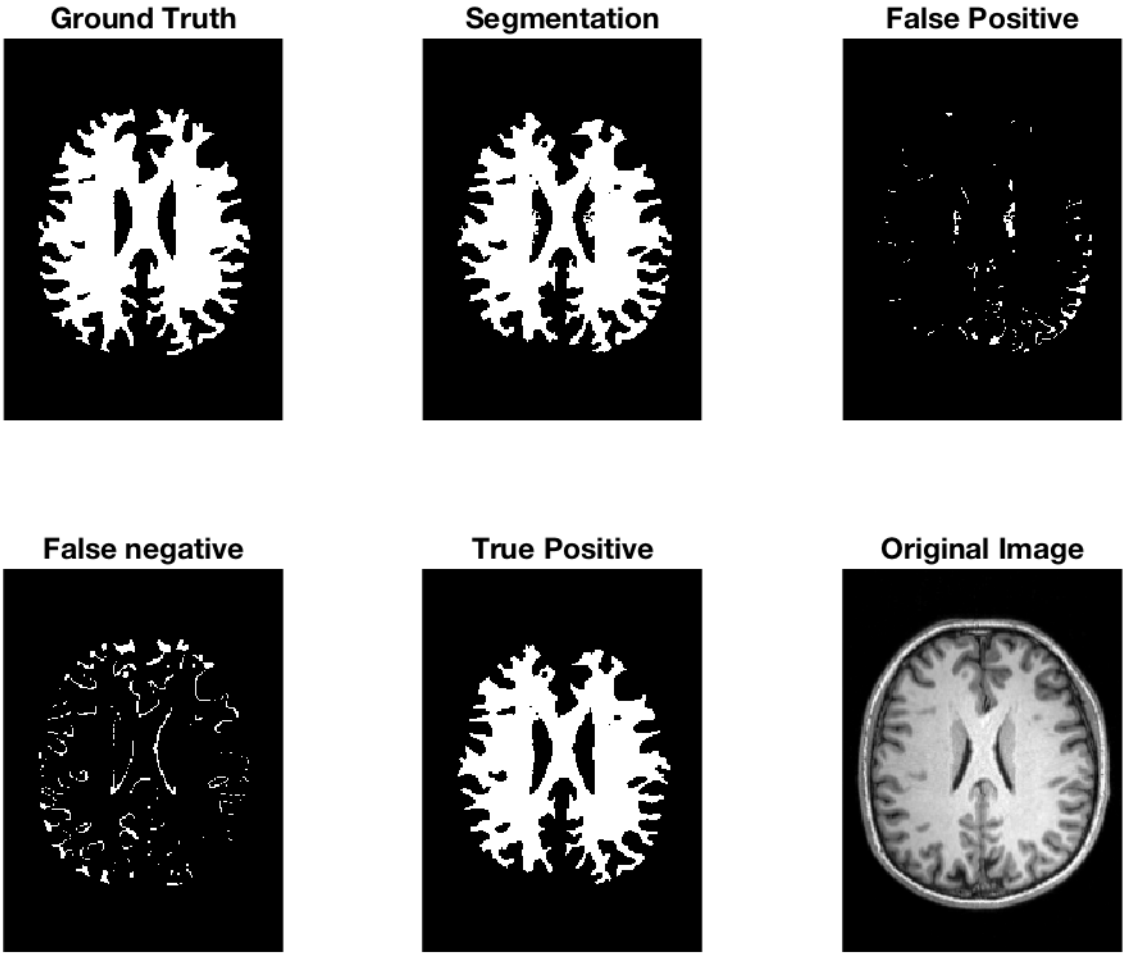

Figure 6.1: Example real-world image with highly non-homogeneous corruption added

6.2 Methodology

6.2.1 Chan-Vese variational Level set

Given the success of the previous method, investigation was carried out as to how to leverage the abilities of the kernel-based clustering methods to deal with pixel inhomogeneities and the level-set methods to accurately and quickly find the object contours. To do this we first reinvestigate the level-set equation shown in eq. (6.1) in the form of the well known Chan-Vese (CV) variational Level set[88].

$$
\begin{aligned}
F(\phi, c_1, c_2) = &\int_{\Omega} |I(x) - c_1|^2 \mathbf{H}(\phi(x)) dx \\
&+ \int_{\Omega} |I(x) - c_2|^2 (1 - \mathbf{H}(\phi(x))) dx \\
&+ v \int_{\Omega} \nabla |\mathbf{H}(\phi(x))| dx
\end{aligned} \tag{6.1}
$$

Here ϕ is the level set function as shown in eq. (5.1), where the zero level of ϕ will be the bounding point for the image domain Ω and $\mathbf{H}$ is the Heavyside function. The aim is that we can split the image domain Ω into two sub-domains Ω_1 and Ω_2. While the first half of the equation, the c_1 and c_2 terms are the for the purpose of fitting the surface evolution to fit the image data, the last part is for regularising the zero level set contour; given that the weight term $v > 0$.

It is important to note that there are some assumption on the success of the CV model, such as it is possible to approximate the image using the constants c_1 and c_2 into the subdomains Ω_2 and Ω_2.

6.2.2 Conditional energy formulation

Because we wish to implement the properties of local clustering into the level set formulation, the most obvious way is to use the c_1 and c_2 terms as local clustering terms, thus we could rewrite eq. (6.1) as eq. (6.2).

$$
\begin{aligned}
F(\phi, c_1, c_2) = &\int_{\Omega} |\mathbf{U}(x) - c_1|^2 \mathbf{H}(\phi(x)) dx \\
&+ \int_{\Omega} |\mathbf{U}(x) - c_2|^2 (1 - \mathbf{H}(\phi(x))) dx \\
&+ v \int_{\Omega} \nabla |\mathbf{H}(\phi(x))| dx
\end{aligned} \tag{6.2}
$$

Where $\mathbf{U}$ is the uncertainty maps for the image found by the FCM algorithm. By using the leveraged fuzzy memberships from the Kernel based Fuzzy clustering

algorithm we are able to bypass the problems faced by normal contour methods. For simplicity from here onwards we will rewrite $U(x)$ simply as U.

We must then conduct optimisation to update $\phi(x)$ by performing gradient decent on the Lagrangian version of eq. (6.2) shown in eq. (6.3).

$$\phi_{t+} = \delta(\phi)\left[(\mathbf{U}-c_1)^2-(\mathbf{U}-c_2)^2-\nu\nabla\frac{\nabla\phi}{|\nabla\phi|}\right] \tag{6.3}$$

Here δ is the delta dirac function. We must then update the centroids c_1 and c_2 by the following eq. (6.4) on each iteration of the algorithm.

$$c_1 = \frac{\int_\Omega \mathbf{U}\mathbf{H}(\phi(x))\mathrm{dx}}{\int_\Omega \mathbf{H}(\phi(x))\mathrm{dx}} \quad , \quad c_2 = \frac{\int_\Omega \mathbf{U}(1-\mathbf{H}(\phi(x))\mathrm{dx})}{\int_\Omega (1-\mathbf{H}(\phi(x))\mathrm{dx})} \tag{6.4}$$

From here the process is the same as shown in algorithm 1 except we need to update it to also include the Level-set formulation to give algorithm 2.

Algorithm 2 Updated FRLS algorithm

procedure OPTIMISE PARAMETERS
    loop:
    Calculate Uncertainty matrix **U**
    $\phi^+ \leftarrow \delta(\phi)\left[(\mathbf{U}-c_1)^2-(\mathbf{U}-c_2)^2-\nu\nabla\frac{\nabla\phi}{|\nabla\phi|}\right]$
    $c_1^+ \leftarrow \frac{\int_\Omega \mathbf{U}\mathbf{H}(\phi(x))\mathrm{dx}}{\int_\Omega \mathbf{H}(\phi(x))\mathrm{dx}}$
    $c_2^+ = \frac{\int_\Omega \mathbf{U}(1-\mathbf{H}(\phi(x))\mathrm{dx})}{\int_\Omega (1-\mathbf{H}(\phi(x))\mathrm{dx})}$
    if $max(\phi^+ - \phi) < \varepsilon$ **then**
        break;
    else
        goto *loop*.
    end if
end procedure

6.3 Experimentation: FRLS Segmentation of the M-FISH image set

For this method, we experimented on the same dataset found in chapter 4: The M-FISH dataset. Given the improved results shown it is a natural development to test this method on a real world dataset. For brevity we will not discuss this dataset again, for reference the reader is directed to chapter 4 on page 28. Similar to the previous experiments, a difficult to segment image was chosen to test the algorithm. Difficult to segment in this case would be one which performs very badly using the traditional methods.

The following experiments were performed using the same subset of images which were described in chapter 4, which is a subset consisting of images which contained highly corrupted and difficult to segment images. As such, this can be seen as a highly tailored and specialised algorithm intended to solve a singular problem of highly corrupted M-FISH images.

Additionally, as well as the normal CR and FR, we introduced new metrics to analyse the performance of the algorithm. Namely, precision, recall, F-score and specificity. All the required values to calculate these metrics and their meaning will be given as follows.

Precision (eq. (6.5)) shows the ratio of correctly segmented pixels compared to the total number of pixels. Thus, a high precision would indicate a lower false positive compared to true positive. While this is useful, for medical imaging we also need to be aware of how many pixels were falsely represented, which leads us into recall.

$$Precision = \frac{TP}{TP+FP} \tag{6.5}$$

Recall eq. (6.6) shows the ratio of correctly segmented pixels to the amount of pixels which were segmented as chromosome pixels; This is an essential measurement in medical imaging. Often a false positive could be almost as bad as a false negative so we must take this into consideration.

$$Recall = \frac{TP}{TP + FN} \tag{6.6}$$

The F-score eq. (6.7) is the weighted average of both the Precision and the Recall. This is specifically useful when dealing with a dataset which has an uneven data-distribution such as the M-FISH image sets.

$$F - Score = \frac{2 * (Recall * Precision)}{(Recall + Precision)} \tag{6.7}$$

Specificity eq. (6.8) can be seen as the true negative rate. Specificity will show a measurement of how many background pixels were correctly segmented compared with how many were falsely identified as chromosome pixels. Overall, while all of the metrics are useful, we would like to see both a high Specificity and Precision when dealing with the difficult to segment images. If there is a situation where one method has a low recall and a high specificity but the other has a high recall but low specificity, we can use the F-score as a deciding factor.

$$Specificity = \frac{TN}{TN + FP} \tag{6.8}$$

6.4 Results

For each set of results, the FRLS algorithm was compared with the KAFCM and IAFCM algorithms. As previous, we found the True positive and False positive values, however, in this experiment we also considered the precision, recall, F-score and specificity.

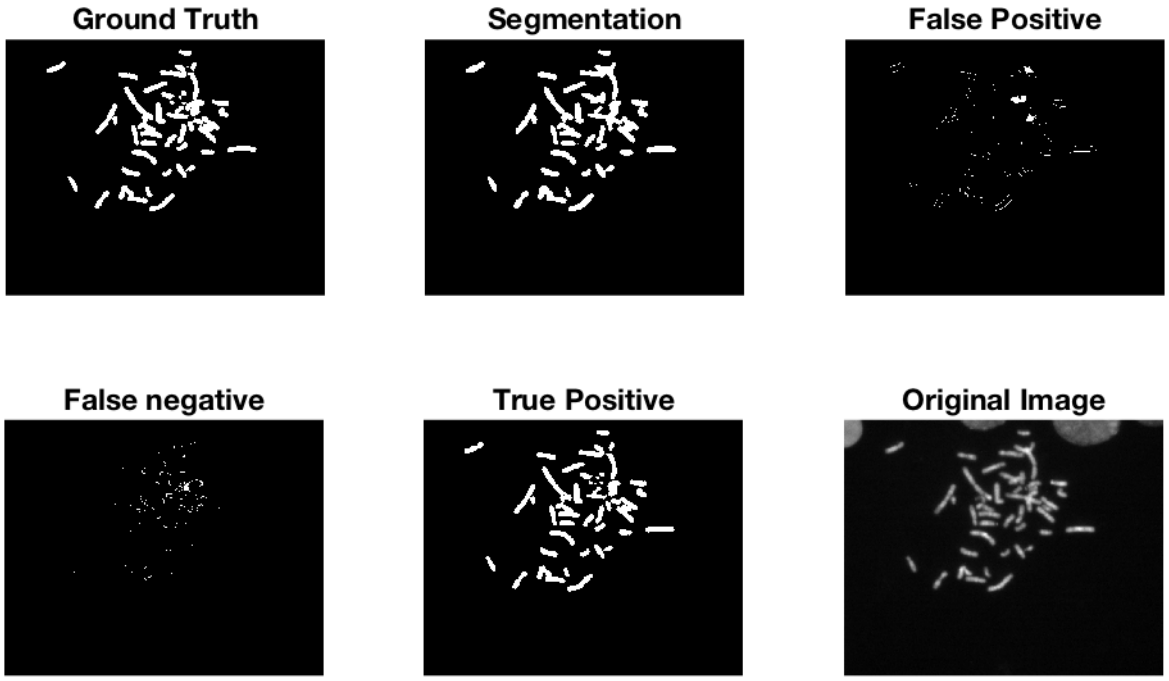

Figure 6.2: Results using FRLS method on Karyotype DAPI channel

Table 6.2: Results for FRLS on DAPI channel

Results on the Dapi channel

Method	CR (%)	FR (%)	Precision	Recall	F-score
KAFCM	98.32	0.96	86.36	98.48	92.03
IAFCM	97.12	0.82	85.21	98.10	91.2
FRLS	96.17	0.36	93.47	94.18	93.82

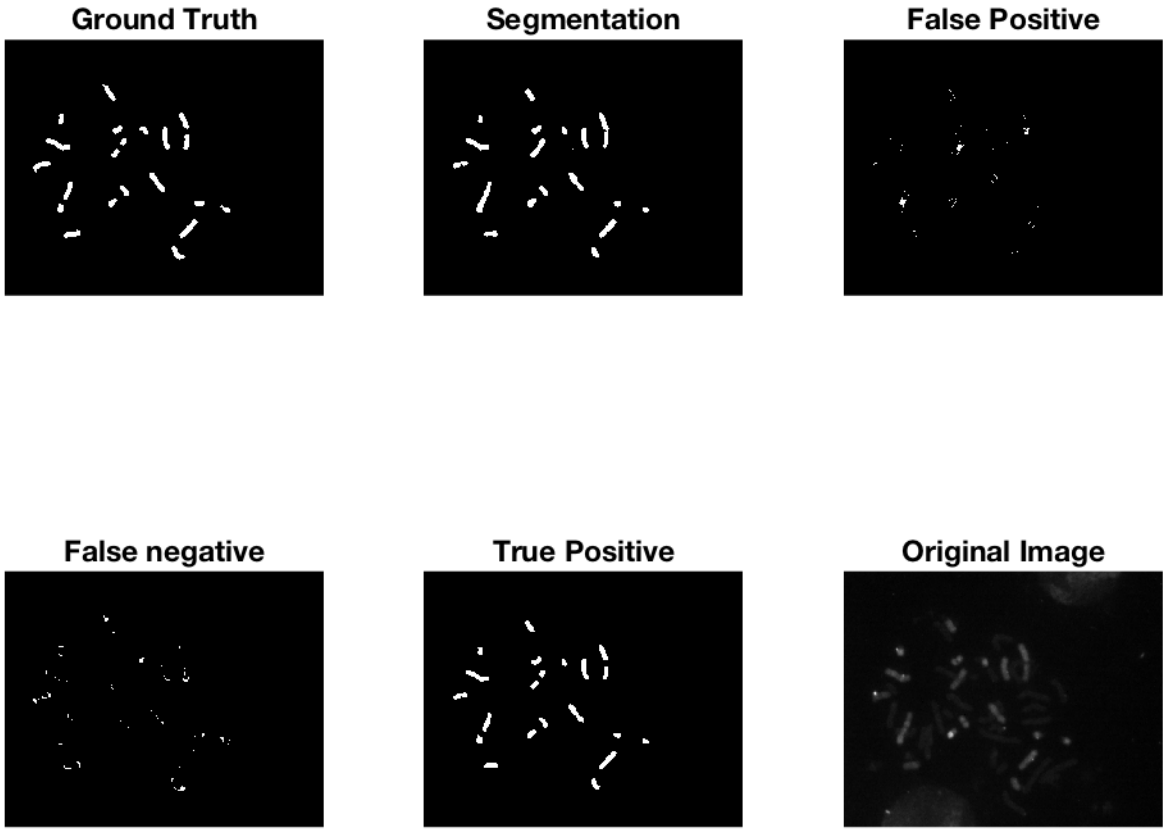

Figure 6.3: Results using FRLS method on Karyotype A channel

Table 6.3: Results for FRLS on Aqua channel

Results on the Aqua channel

Method	CR (%)	FR (%)	Precision	Recall	F-score	Specificity
KAFCM	44.01	0.23	78.14	44.01	56.31	99.77
IAFCM	31.26	3.45	66.25	41.27	50.86	99.12
FRLS	94.18	0.36	93.47	94.18	93.82	99.64

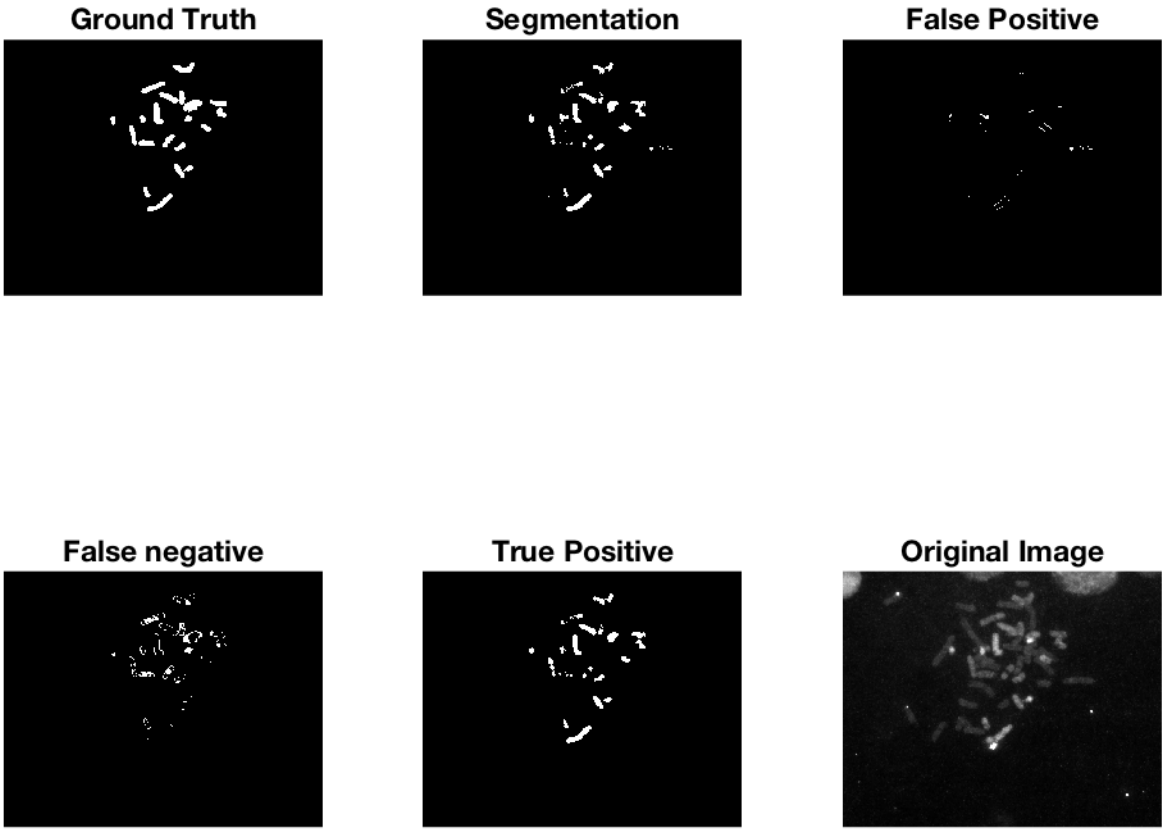

Figure 6.4: Results using FRLS on Karyotype Green channel

Table 6.4: Results for FRLS on Green channel

Results for FRLS on Green channel

Method	CR (%)	FR (%)	Precision	Recall	F-score	Specificity
KAFCM	41.42	0.86	49.43	40.41	44.46	99.14
IAFCM	45.62	3.91	47.11	39.88	43.19	99.03
FRLS	63.23	0.13	90.68	63.96	75.01	99.87

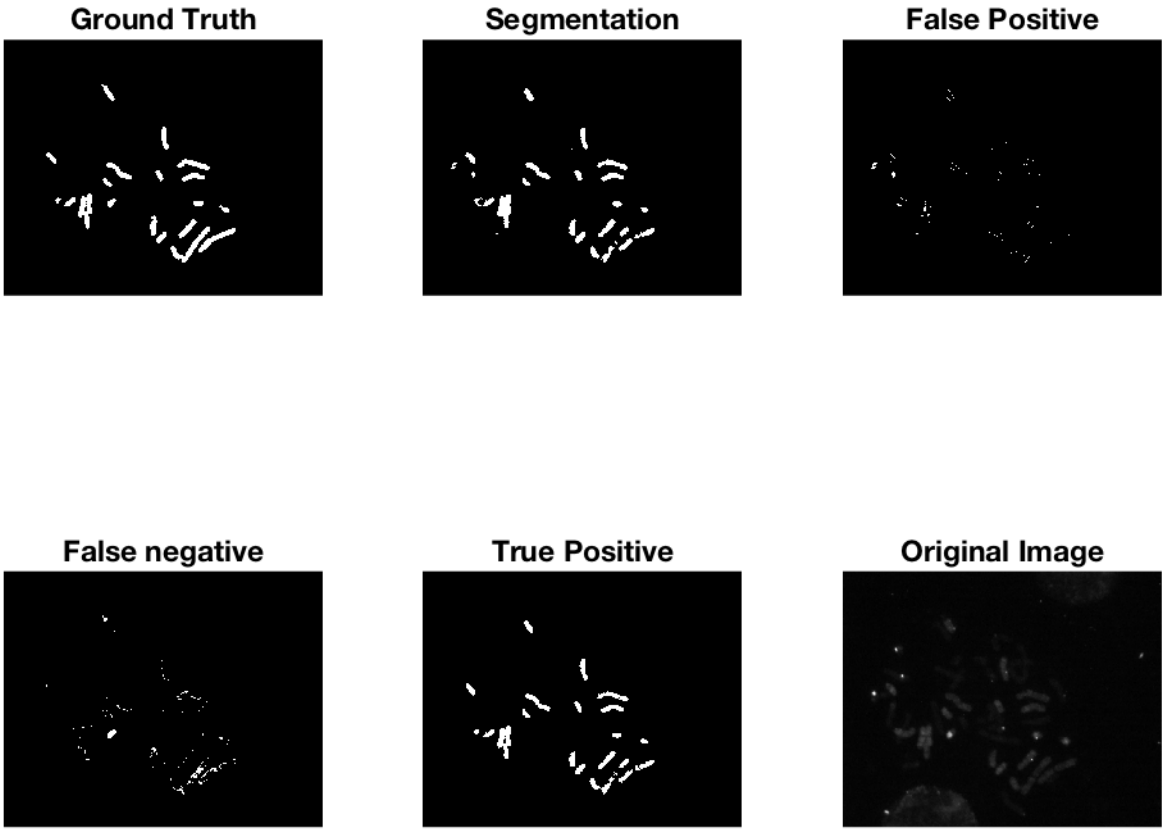

Figure 6.5: Results using Chapter 6 method on Karyotype Gold channel

Table 6.5: Results for FRLS on Gold channel

Results for FRLS on Gold channel

Method	CR (%)	FR (%)	Precision	Recall	F-score	Specificity
KAFCM	48.14	0.49	73.59	46.62	57.08	99.57
IAFCM	46.22	0.61	69.41	47.10	56.12	99.32
FRLS	82.27	0.21	90.89	81.26	85.80	99.79

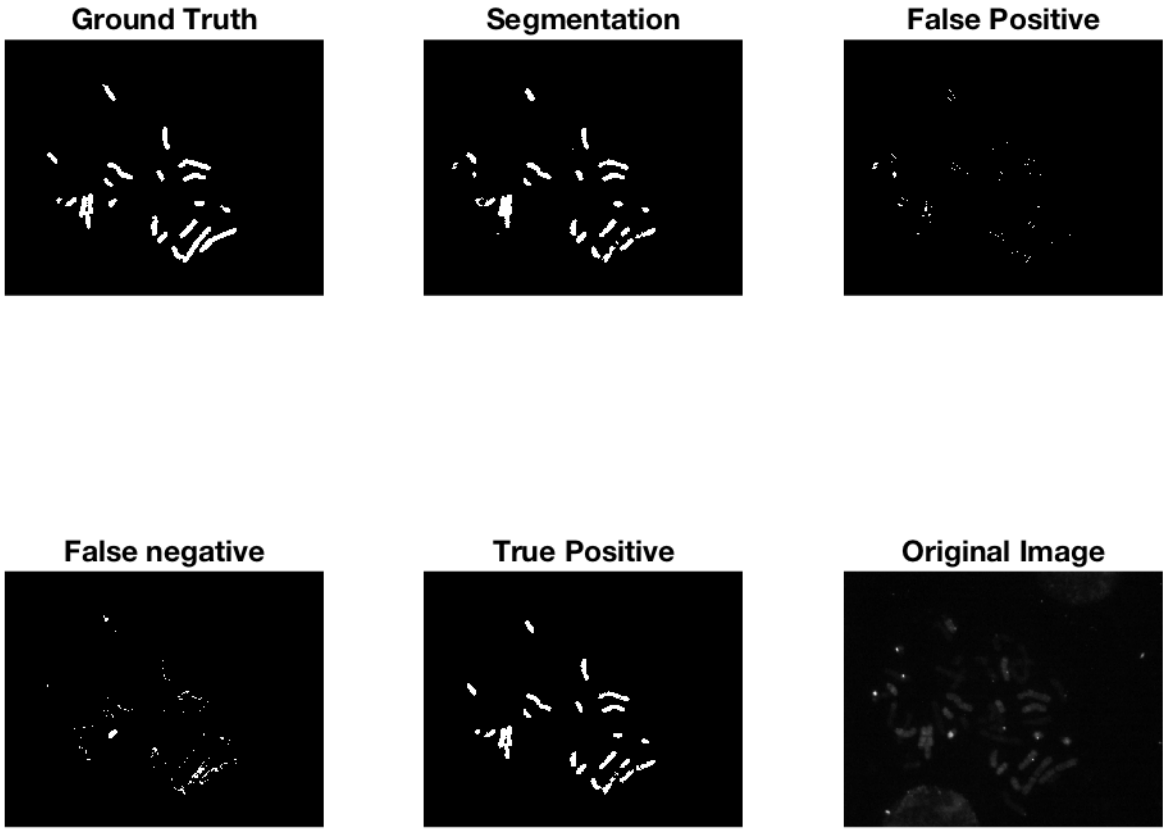

Figure 6.6: Results using FRLS on Karyotype Red channel

Table 6.6: Results for FRLS on Red channel

Results for FRLS on Red channel

Method	CR (%)	FR (%)	Precision	Recall	F-score	Specificity
KAFCM	45.72	0.99	55.07	45.83	50.03	99.01
IAFCM	31.45	4.32	32.14	41.75	36.32	98.05
FRLS	92.12	0.40	85.87	92.05	88.85	99.60

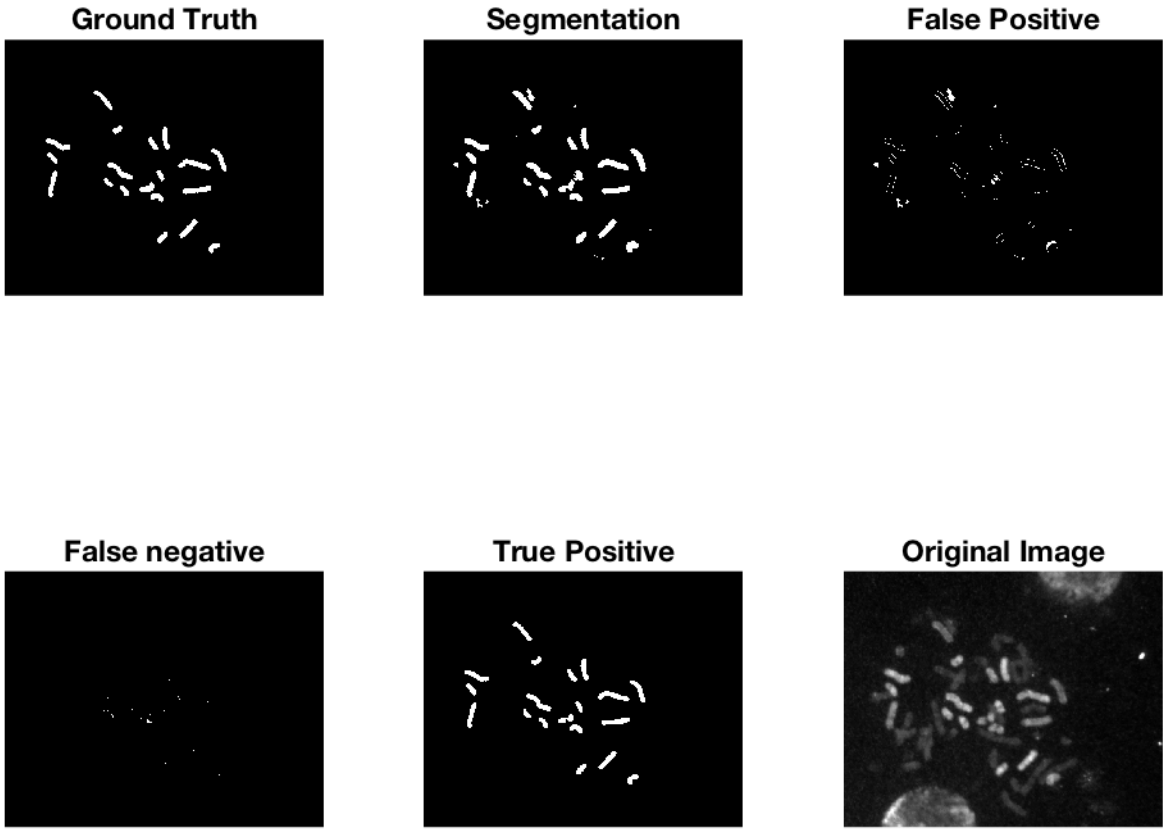

Figure 6.7: Results using FRLS on Karyotype Far Red channel

Table 6.7: Results for FRLS on Far Red channel

Results for FRLS on Far Red channel

Method	CR (%)	FR (%)	Precision	Recall	F-score	Specificity
KAFCM	11.10	2.13	12.56	11.87	12.20	98.18
IAFCM	7.82	9.82	10.44	7.67	8.84	97.92
FRLS	74.68	0.10	93.87	74.68	83.18	99.90

It can be seen from the results, that for all of the colour channels the FRLS algorithm performs significantly better in terms of its F-score, meaning it has a high true positive and and low false negative results. This is ideal for this type of medical image segmentation.

6.5 Discussion

This chapter presented an algorithm based on both the KAFCM and Chan-Vese variational level-set. Additionally, new metrics were introduced to analyse the algorithms performance, namely the Recall, Precision, Specificity and F-score. The experiments were performed on the difficult to segment subset of the M-FISH image dataset which was discussed previously in chapter 4. The algorithm showed a strong performance when compared to the KAFCM and IAFCM algorithms, outperforming them all for each of the image channels.

Observing the results in table 6.2, the F-scores of the segmentations are relatively similar, but this is to be expected as the DAPI channel is, in general, the easiest to segment due to the more uniform distribution of pixel intensities. However, observing the results in tables 6.3, 6.4, 6.5, 6.6 and 6.7 The proposed method shows a higher F-score for all results. Observing the results in table 6.7, we can see that the f-score is 70.98% higher than the KAFCM algorithm, showing that the proposed method has a much stronger capability of overcoming the corruptions within the image. This strong capability is mostly due to the algorithms ability to overcome the problems of the uneven pixel distributions caused by the uneven hybridisation; this can be observed in fig. 6.7 where there are some chromosomes which are not fluorescing as brightly as others. However, while the false negative is very low, the CR is still relatively low also; this is not a good situation for a segmentation algorithm is we want to be able to achieve full automation.

While the proposed system is useful for this specific application, there is a potential and interest to see how well the proposed classifier can work on other datasets. The proposed method does show a strong ability to overcome image corruptions, but it has only been tested on a specific type of publicly available dataset. To prove it as a general solution more data would be needed. Furthermore, it is

currently unknown how well it would perform on additional types of real-world corruptions. Thus, further research is needed on improving this aspect of the algorithm, and also investigations on how well this method could work on other datasets need to be carried out. In future work, we would discover how general the algorithm is when dealing with other datasets, not exclusive to medical imaging.

Chapter 7

Conclusions and Suggestions for Future Research

This chapter concludes the thesis and provides the future research directions for this topic.

7.1 Conclusions

In this thesis, unsupervised pattern recognition techniques are used to properly segment highly corrupted medical image data. A set of algorithms are developed to improve the accuracy of segmentation taking into consideration the intrinsic corruptions of the images. Additionally the methods used taking into consideration the usual concerns with medical imaging such as small sample sizes, and requiring good explainability. The findings of this study are summarised as follows:

An novel algorithm KAFCM based on FCM, modified to consider local spatial data and then projected into the kernel space to improve segmentation accuracy. Experimental results demonstrate the effectiveness of the proposed method in tackling the inhomogeneities in pixel intensities as well as the image artefacts by competing well compared to other methods used on this dataset. This unsupervised method requires no minimum sample size and is readily explainable to medical practitioners,

thus is could be suitable for application on real world medical images.

The hybrid LRLS, Local-region clustering informed level-set algorithm based on both FCM and level set is developed using both methods in series with one another. This has the advantage of removing the problems which faced each of the methods individually as they compliment one anothers weaknesses. This method was tested on both real world and synthetic images and showed a good result compared to other competing works and also to the KAFCM algorithm.

The FRLS, Fuzzy region based level set follows the core idea both the KAFCM and the LR-level set by further fusing the two methods. This method leverages the probabilistic fuzzy uncertainties from the KAFCM into the input of the FRLS, calculating both in parallel. This allows the energy function pushing the level set front to be influenced by the intrinsic data found at the pixel level. This allows it to overcome both the pixel artefacts and the intensity inhomogeneities whilst maintaining the smooth curves.

Each of the proposed unsupervised pattern recognition methods has been applied to real world medical images and the results demonstrate that the proposed methods result in an overall improvement segmentation. The fundamental problems facing segmenting these medical images such as small datasets, image corruptions and explainability is possible to be overcome without the need of large computational power. These results on real datasets demonstrate the potential of the investigated methods and give rise to further study.

7.2 Suggestions for Future Research

This thesis identifies the following directions as future work:

(a) Further investigation into what other datasets would be suitable for the developed methods will be investigated. Specifically MRI image data should be

investigated.

(b) A study into using deep-learning to supplement these methods, and an investigation as to the potential scalability with small datasets and how explainable the results can be.

(c) The development of a fully automated system which required minimal human interaction for segmenting M-FISH karyotype images and classifying chromosome deformities.

Bibliography

[1] Dzung L Pham and Jerry L Prince. An adaptive fuzzy C-means algorithm for image segmentation in the presence of intensity inhomogeneities. *Pattern Recognition Letters*, 1999.

[2] D. L. Pham and J. L. Prince. Adaptive fuzzy segmentation of magnetic resonance images. *IEEE Transactions on Medical Imaging*, 18(9):737–752, 9 1999. ISSN 0278-0062. doi: 10.1109/42.802752.

[3] Sandra González-Villà, Arnau Oliver, Sergi Valverde, Liping Wang, Reyer Zwiggelaar, and Xavier Lladó. A review on brain structures segmentation in magnetic resonance imaging. *Artificial Intelligence in Medicine*, 73:45–69, 10 2016.

[4] Charles R Meyer, Peyton H Bland, and James Pipe. Retrospective Correction of MRI Amplitude Inhomogeneities. In *Computer Vision, Virtual Reality and Robotics in Medicine*, pages 513–522. Springer Berlin Heidelberg, Berlin, Heidelberg, 1995.

[5] Changyang Li, Xiuying Wang, S Eberl, M Fulham, and D D Feng. Robust Model for Segmenting Images With/Without Intensity Inhomogeneities. *IEEE Transactions on Image Processing*, 22(8):3296, 2013.

[6] S K Adhikari, J K Sing, and D K Basu. Bias field estimation and segmenta-

tion of MRI images using a Spatial Fuzzy C-means algorithm. In *2016 2nd International Conference on Control, Instrumentation, Energy & Communication (CIEC) IS - SN - VO - VL -*, pages 158–162, 2016.

[7] H. Cao, H. W. Deng, and Y. P. Wang. Segmentation of m-fish images for improved classification of chromosomes with an adaptive fuzzy c-means clustering algorithm. *IEEE Transactions on Fuzzy Systems*, 20(1):1–8, 2 2012. ISSN 1063-6706. doi: 10.1109/TFUZZ.2011.2160025.

[8] Keh-Shih Chuang, Hong-Long Tzeng, Sharon Chen, Jay Wu, and Tzong-Jer Chen. Fuzzy c-means clustering with spatial information for image segmentation. *Computerized Medical Imaging and Graphics*, 30(1):9–15, 1 2006. ISSN 0895-6111. doi: 10.1016/j.compmedimag.2005.10.001.

[9] Jamuna Kanta Sing, Sudip Kumar Adhikari, and Dipak Kumar Basu. A modified fuzzy C-means algorithm using scale control spatial information for MRI image segmentation in the presence of noise. *Journal of Chemometrics*, 29(9):492–505, 9 2015.

[10] J G Sled, A P Zijdenbos, and A C Evans. A nonparametric method for automatic correction of intensity nonuniformity in MRI data. *IEEE Transactions on Medical Imaging*, 17(1):87–97, 1998.

[11] W M Wells, W E L Grimson, R Kikinis, and F A Jolesz. Adaptive Segmentation of MRI Data. *IEEE Transactions on Medical Imaging*, 15(4):429–442, 1996.

[12] R Guillemaud and M Brady. Estimating the bias field of MR images. *IEEE Transactions on Medical Imaging*, 16(3):238–251, 6 1997.

[13] Nooshin Nabizadeh and Miroslav Kubat. Brain tumors detection and segmentation in MR images: Gabor wavelet vs. statistical features. *Computers & Electrical Engineering*, 45:286–301, 7 2015.

[14] Stefan Bauer, Roland Wiest, Lutz-P Nolte, and Mauricio Reyes. A survey of mri-based medical image analysis for brain tumor studies. *Physics in Medicine & Biology*, 58(13):R97, 2013.

[15] A Kassner and RE Thornhill. *Texture analysis: a review of neurologic MR imaging applications*, volume 31. Am Soc Neuroradiology, 2010.

[16] Ahmed Kharrat, Mohamed BenMessaoud, and Mohamed Abid. Brain tumour diagnostic segmentation based on optimal texture features and support vector machine classifier. *International Journal of Signal and Imaging Systems Engineering*, 7(2):65, 2014.

[17] V Lepetit, P Lagger, and P Fua. Randomized Trees for Real-Time Keypoint Recognition. In *2005 IEEE Computer Society Conference on Computer Vision and Pattern Recognition (CVPR'05)*, pages 775–781. IEEE, 2005.

[18] Jamie Shotton, Toby Sharp, Alex Kipman, Andrew Fitzgibbon, Mark Finocchio, Andrew Blake, Mat Cook, and Richard Moore. Real-time human pose recognition in parts from single depth images. *Communications of the ACM*, 56(1):116–124, 1 2013.

[19] M Schmidt, I Levner, R Greiner, A Murtha, and A Bistritz. Segmenting Brain Tumors using Alignment-Based Features. In *Fourth International Conference on Machine Learning and Applications (ICMLA'05)*, pages 215–220. IEEE, 2005.

[20] S Ahmed, K M Iftekharuddin, and A Vossough. Efficacy of Texture, Shape, and Intensity Feature Fusion for Posterior-Fossa Tumor Segmentation in MRI. *IEEE Transactions on Information Technology in Biomedicine*, 15(2): 206–213, 2011.

[21] A Rajendran and R Dhanasekaran. Fuzzy Clustering and Deformable Model for Tumor Segmentation on MRI Brain Image: A Combined Approach. *Procedia Engineering*, 30:327–333, 2012.

[22] Tao Wang, Irene Cheng, Anup Basu, et al. Fluid vector flow and applications in brain tumor segmentation. *IEEE Transactions on Biomedical Engineering*, 56(3):781–789, 2009.

[23] M Lorenzi, N Ayache, G B Frisoni, and X Pennec. LCC-Demons: a robust and accurate symmetric diffeomorphic registration algorithm. *LCC-Demons: a robust and accurate symmetric diffeomorphic registration algorithm*, 2013.

[24] Tim McInerney and Demetri Terzopoulos. Deformable models in medical image analysis: a survey. *Medical Image Analysis*, 1(2):91–108, 6 1996.

[25] S Ho, E Bullitt, and G Gerig. Level-set evolution with region competition: automatic 3-D segmentation of brain tumors. In *16th International Conference on Pattern Recognition*, pages 532–535. IEEE Comput. Soc, 2002.

[26] Jan Rexilius, Horst K Hahn, Jan Klein, Markus G Lentschig, and Heinz-Otto Peitgen. Multispectral brain tumor segmentation based on histogram model adaptation. *Medical Imaging*, 6514:65140V–65140V–10, 3 2007.

[27] Vida Harati, Rasoul Khayati, and Abdolreza Farzan. Fully automated tumor segmentation based on improved fuzzy connectedness algorithm in brain MR images. *Computers in biology and medicine*, 41(7):483–492, 7 2011.

[28] Lothar R Schad, Stefan Blüml, and Ivan Zuna. IX. MR tissue characterization of intracranial tumors by means of texture analysis. *Magnetic resonance imaging*, 11(6):889–896, 1 1993.

[29] WE Phillips II, RP Velthuizen, S Phuphanich, LO Hall, LP Clarke, and ML Silbiger. Application of fuzzy c-means segmentation technique for tissue differentiation in mr images of a hemorrhagic glioblastoma multiforme. *Magnetic resonance imaging*, 13(2):277–290, 1995.

[30] M Vaidyanathan, L P Clarke, R P Velthuizen, S Phuphanich, A M Bensaid, L O Hall, J C Bezdek, H Greenberg, A Trotti, and M Silbiger. Comparison of supervised MRI segmentation methods for tumor volume determination during therapy. *Magnetic resonance imaging*, 13(5):719–728, 1 1995.

[31] M C Clark, L O Hall, D B Goldgof, R Velthuizen, F R Murtagh, and M S Silbiger. Automatic tumor segmentation using knowledge-based techniques. *IEEE Transactions on Medical Imaging*, 17(2):187–201, 4 1998.

[32] Lynn M Fletcher-Heath, Lawrence O Hall, Dmitry B Goldgof, and F Reed Murtagh. Automatic segmentation of non-enhancing brain tumors in magnetic resonance images. *Artificial Intelligence in Medicine*, 21(1-3):43–63, 1 2001.

[33] Hongmin Cai, Ragini Verma, Yangming Ou, Seung-koo Lee, Elias Melhem, and Christos Davatzikos. Probabilistic Segmentation of Brain Tumors Based on Multi-modality Magnetic Resonance Images. In *2007 4th IEEE International Symposium on Biomedical Imaging: From Nano to Macro*, pages 600–603. IEEE, 2007.

[34] Ragini Verma, Evangelia I Zacharaki, Yangming Ou, Hongmin Cai, Sanjeev

Chawla, Seung-koo Lee, Elias R Melhem, Ronald Wolf, and Christos Davatzikos. Multiparametric Tissue Characterization of Brain Neoplasms and Their Recurrence Using Pattern Classification of MR Images. *Academic radiology*, 15(8):966–977, 8 2008.

[35] Su Ruan, Stephane Lebonvallet, Abderrahim Merabet, and Jean-marc Constans. Tumor Segmentation from a Multispectral MRI Images by Using Support Vector Machine Classification. In *2007 4th IEEE International Symposium on Biomedical Imaging: From Nano to Macro*, pages 1236–1239. IEEE, 2007.

[36] Su Ruan, Nan Zhang, Qingmin Liao, and Yuemin Zhu. Image fusion for following-up brain tumor evolution. In *2011 8th IEEE International Symposium on Biomedical Imaging (ISBI 2011)*, pages 281–284. IEEE, 2011.

[37] Todd R Jensen and Kathleen M Schmainda. Computer-aided detection of brain tumor invasion using multiparametric MRI. *Journal of Magnetic Resonance Imaging*, 30(3):481–489, 9 2009.

[38] Darko Zikic, Ben Glocker, Ender Konukoglu, Antonio Criminisi, C Demiralp, J Shotton, O M Thomas, T Das, R Jena, and S J Price. Decision Forests for Tissue-Specific Segmentation of High-Grade Gliomas in Multi-channel MR. In *Medical Image Computing and Computer-Assisted Intervention – MICCAI 2012*, pages 369–376. Springer Berlin Heidelberg, Berlin, Heidelberg, 10 2012.

[39] Michael R Kaus, Simon K Warfield, Arya Nabavi, Peter M Black, Ferenc A Jolesz, and Ron Kikinis. Automated Segmentation of MR Images of Brain Tumors. *Radiology*, 218(2):586–591, 2 2001.

[40] Nathan Moon, Elizabeth Bullitt, Koen van Leemput, and Guido Gerig. Automatic Brain and Tumor Segmentation. In *Medical Image Computing and Computer-Assisted Intervention — MICCAI 2002*, pages 372–379. Springer Berlin Heidelberg, Berlin, Heidelberg, 9 2002.

[41] Marcel Prastawa, Elizabeth Bullitt, Nathan Moon, Koen van Leemput, and Guido Gerig. Automatic brain tumor segmentation by subject specific modification of atlas priors1. *Academic radiology*, 10(12):1341–1348, 12 2003.

[42] J Lafferty, A McCallum, and F Pereira. Conditional random fields: Probabilistic models for segmenting and labeling sequence data. 2001.

[43] Sanjiv Kumar and Martial Hebert. Discriminative Random Fields. *International Journal of Computer Vision*, 68(2):179–201, 2006.

[44] L Zhao, W Wu, and J J Corso. Semi-automatic brain tumor segmentation by constrained mrfs using structural trajectories. *Semi-automatic brain tumor segmentation by constrained mrfs using structural trajectories*, 2013.

[45] Neil Birkbeck, Dana Cobzas, Martin Jägersand, Albert Murtha, and Tibor Kesztyues. An interactive graph cut method for brain tumor segmentation. In *2009 Workshop on Applications of Computer Vision (WACV*, pages 1–7. IEEE, 2009.

[46] Andac Hamamci, Nadir Kucuk, Kutlay Karaman, Kayihan Engin, and Gozde Unal. Tumor-Cut: Segmentation of Brain Tumors on Contrast Enhanced MR Images for Radiosurgery Applications. *IEEE Transactions on Medical Imaging*, 31(3):790–804, 2012.

[47] Dana Cobzas, Neil Birkbeck, Mark W Schmidt, Martin Jägersand, and Al-

bert Murtha. 3D Variational Brain Tumor Segmentation using a High Dimensional Feature Set. *ICCV*, 2007.

[48] Stefan Bauer, Nicole Porz, Raphael Meier, Alessia Pica, Johannes Slotboom, Roland Wiest, and Mauricio Reyes. Interactive segmentation of MR images from brain tumor patients. *ISBI*, 2014.

[49] Stefan Bauer, Roland Wiest, Lutz-P Nolte, and Mauricio Reyes. A survey of MRI-based medical image analysis for brain tumor studies. *Physics in medicine and biology*, 58(13):R97, 2013.

[50] Gloria P Mazzara, Robert P Velthuizen, James L Pearlman, Harvey M Greenberg, and Henry Wagner. Brain tumor target volume determination for radiation treatment planning through automated MRI segmentation. *International Journal of Radiation Oncology*, 59(1):300–312, 5 2004.

[51] E Schrock, S du Manoir, T Veldman, B Schoell, J Wienberg, M A Ferguson-Smith, Y Ning, D H Ledbetter, I Bar-Am, D Soenksen, Y Garini, and T Ried. Multicolor Spectral Karyotyping of Human Chromosomes. *Science*, 273 (5274):494–497, 7 1996.

[52] Michael R Speicher, Stephen Gwyn Ballard, and David C Ward. Karyotyping human chromosomes by combinatorial multi-fluor FISH. *Nature genetics*, 12 (4):368, 1996.

[53] M P Sampat, A C Bovik, J K Aggarwal, and K R Castleman. Supervised parametric and non-parametric classification of chromosome images. *Pattern recognition*, 38(8):1209, 2005.

[54] W C Schwartzkopf, A C Bovik, and B L Evans. Maximum-likelihood tech-

niques for joint segmentation-classification of multispectral chromosome images. *IEEE transactions on medical imaging*, 24(12):1593, 2005.

[55] Y P Wang and Ashok Kumar Dandpat. Classification of M-FISH images using fuzzy C-means clustering algorithm and normalization approaches. In *Signals, Systems and Computers, 2004. Conference Record of the Thirty-Eighth Asilomar Conference on*. IEEE, 2004.

[56] M Wang, T Z Huang, J Li, and Y P Wang. A patch-based tensor decomposition algorithm for M-FISH image classification. *Cytometry Part A*, 2016.

[57] Y P Wang and A K Dandpat. Classification of multi-spectral florescence in situ hybridization images with fuzzy clustering and multiscale feature selection. *2006 IEEE International Workshop on Genomic Signal Processing and Statistics*, 2006.

[58] AWC Liew, SH Leung, and WH Lau. Fuzzy image clustering incorporating spatial continuity. *IEE Proceedings-Vision, Image and Signal Processing*, 147(2):185–192, 2000.

[59] Yu-Ping Wang. Detection of chromosomal abnormalities with multi-color fluorescence in situ hybridization (M-FISH) imaging and multi-spectral wavelet analysis. *2008 30th Annual International Conference of the IEEE Engineering in Medicine and Biology Society*, 2008.

[60] Hyohoon Choi, A C Bovik, and K R Castleman. Feature Normalization via Expectation Maximization and Unsupervised Nonparametric Classification For M-FISH Chromosome Images. *IEEE transactions on medical imaging*, 27(8):1107, 2008.

[61] S Derivaux, G Forestier, C Wemmert, and S Lefèvre. Supervised image segmentation using watershed transform, fuzzy classification and evolutionary computation. *Pattern Recognition Letters*, 31(15):2364–2374, 2010.

[62] Jingyao Li, Dongdong Lin, and Yu-Ping Wang. Segmentation of Multicolor Fluorescence In-Situ Hybridization (M-FISH) image using an improved Fuzzy C-means clustering algorithm while incorporating both spatial and spectral information. *2015 IEEE International Conference on Bioinformatics and Biomedicine (BIBM)*, 2015.

[63] P. S. Karvelis, D. I. Fotiadis, A. Tzallas, and I. Georgiou. Region based segmentation and classification of multispectral chromosome images. In *Twentieth IEEE International Symposium on Computer-Based Medical Systems (CBMS'07)*, pages 251–256, 6 2007. doi: 10.1109/CBMS.2007.92.

[64] M Girolami. Mercer kernel-based clustering in feature space. *IEEE Transactions on Neural Networks*, 13(3):780, 2002.

[65] Hongbin Shen, Jie Yang, Shitong Wang, and Xiaojun Liu. Attribute weighted mercer kernel based fuzzy clustering algorithm for general non-spherical datasets. *Soft Computing*, 10(11):1061, 2006.

[66] D Q Zhang and S C Chen. Clustering incomplete data using kernel-based fuzzy c-means algorithm. *Neural Processing Letters*, 18(3):155–162, 2003. ISSN 1573-773X. doi: 10.1023/B:NEPL.0000011135.19145.1b.

[67] D Q Zhang and S C Chen. A novel kernelized fuzzy c-means algorithm with application in medical image segmentation. *Artificial Intelligence in Medicine*, 2004.

[68] Trong Hop Dang, Long Thanh Ngo, and Witold Pedrycz. Multiple Kernel Based Collaborative Fuzzy Clustering Algorithm. *Lecture Notes in Computer Science*, 2016.

[69] Dzung Dinh Nguyen, Long Thanh Ngo, Long The Pham, and Witold Pedrycz. Towards hybrid clustering approach to data classification - Multiple kernels based interval-valued Fuzzy C-Means algorithms. *Fuzzy Sets and Systems*, 2015.

[70] D L Pham. Spatial models for fuzzy clustering. *Computer vision and image understanding*, 2001.

[71] AWC Liew and H Yan. An adaptive spatial fuzzy clustering algorithm for 3-D MR image segmentation. *IEEE transactions on medical imaging*, 2003.

[72] Zhimin Wang, Qing Song, Yeng Chai Soh, and Kang Sim. An adaptive spatial information-theoretic fuzzy clustering algorithm for image segmentation. *Computer Vision and Image Understanding*, 2013.

[73] S Chen and D Zhang. Robust image segmentation using FCM with spatial constraints based on new kernel-induced distance measure. *IEEE Transactions on Systems*, 2004.

[74] Yu-Ping Wang. Detection of chromosomal abnormalities with multi-color fluorescence in situ hybridization (M-FISH) imaging and multi-spectral wavelet analysis. *2008 30th Annual International Conference of the IEEE Engineering in Medicine and Biology Society*, 2008.

[75] W Pedrycz and J Waletzky. Fuzzy clustering with partial supervision. *Fuzzy Sets and Systems*, 157(13):1733, 1997.

[76] Jingyao Li, Dongdong Lin, and Yu-Ping Wang. Segmentation of Multicolor Fluorescence In-Situ Hybridization (M-FISH) image using an improved Fuzzy C-means clustering algorithm while incorporating both spatial and spectral information. *2015 IEEE International Conference on Bioinformatics and Biomedicine (BIBM)*, 2015.

[77] M. Gong, Y. Liang, J. Shi, W. Ma, and J. Ma. Fuzzy c-means clustering with local information and kernel metric for image segmentation. *IEEE Transactions on Image Processing*, 22(2):573–584, 2 2013. ISSN 1057-7149. doi: 10.1109/TIP.2012.2219547.

[78] Y A Tolias and S M Panas. On applying spatial constraints in fuzzy image clustering using a fuzzy rule-based system. *IEEE Signal Processing Letters*, 5(10):245, 1998.

[79] Y. A. Tolias and S. M. Panas. Image segmentation by a fuzzy clustering algorithm using adaptive spatially constrained membership functions. *IEEE Transactions on Systems, Man, and Cybernetics - Part A: Systems and Humans*, 28(3):359–369, 5 1998. ISSN 1083-4427. doi: 10.1109/3468.668967.

[80] Hongbin Shen, Jie Yang, Shitong Wang, and Xiaojun Liu. Attribute weighted mercer kernel based fuzzy clustering algorithm for general non-spherical datasets. *Soft Computing*, 10(11):1061–1073, 2006.

[81] M P Sampat, A C Bovik, J K Aggarwal, and K R Castleman. Supervised parametric and non-parametric classification of chromosome images. *Pattern Recognition*, 38(8):1209, 2005.

[82] EDMS Schrock, S Du Manoir, T Veldman, B Schoell, et al. Multicolor spectral karotyping of human chromosomes. *Science*, 273(5274):494, 1996.

[83] Hyohoon Choi, A C Bovik, and K R Castleman. Feature Normalization via Expectation Maximization and Unsupervised Nonparametric Classification For M-FISH Chromosome Images. *IEEE Transactions on Medical Imaging*, 27(8):1107, 2008.

[84] Jim Graham and Jim Piper. Automatic karyotype analysis. In *Chromosome Analysis Protocols*, pages 141–185. Springer, 1994.

[85] Tony F Chan and Luminita A Vese. Active contours without edges. *IEEE Transactions on image processing*, 10(2):266–277, 2001.

[86] A Tsai, A Yezzi, and A S Willsky. Curve evolution implementation of the Mumford-Shah functional for image segmentation, denoising, interpolation, and magnification. *IEEE Transactions on Image Processing*, 10(8):1169, 2001.

[87] D Mumford and J Shah. Optimal approximations by piecewise smooth functions and associated variational problems. *Communications on Pure and Applied Mathematics*, 42(5):577, 1989.

[88] Luminita A Vese and Tony F Chan. A Multiphase Level Set Framework for Image Segmentation Using the Mumford and Shah Model. *International journal of computer vision*, 2002.

[89] M Kass, A Witkin, and D Terzopoulos. Snakes: Active contour models. *Snakes: Active contour models*, 1(4):321–331, 1988.

[90] Vicent Caselles, Ron Kimmel, and Guillermo Sapiro. Geodesic active contours. *International Journal of Computer Vision*, 1997.

[91] Jin Zhou, CL Philip Chen, Long Chen, and Han-Xiong Li. A collaborative fuzzy clustering algorithm in distributed network environments. *IEEE Transactions on Fuzzy Systems*, 22(6):1443–1456, 2014.

[92] Li Chen, Yue Zhou, Yonggang Wang, and Jie Yang. GACV: Geodesic-Aided C-V method. *Pattern Recognition*, 39(7):1391–1395, 2006. ISSN 00313203. doi: 10.1016/j.patcog.2006.01.017.

[93] Keyan Ding, Linfang Xiao, and Guirong Weng. Active contours driven by region-scalable fitting and optimized Laplacian of Gaussian energy for image segmentation. *Signal Processing*, 134(50):224–233, 2017. ISSN 01651684. doi: 10.1016/j.sigpro.2016.12.021.

[94] Kaihua Zhang, Huihui Song, and Lei Zhang. Active contours driven by local image fitting energy. *Pattern Recognition*, 43(4):1199–1206, 2010. ISSN 0031-3203. doi: https://doi.org/10.1016/j.patcog.2009.10.010.

[95] Qi Ge, Liang Xiao, Jun Zhang, and Zhi Hui Wei. An improved region-based model with local statistical features for image segmentation. *Pattern Recognition*, 45(4):1578–1590, 2012. ISSN 0031-3203. doi: https://doi.org/10.1016/j.patcog.2011.09.008.

[96] Qiang Zheng, Enqing Dong, Zhulou Cao, Wenyan Sun, and Zhenguo Li. Active contour model driven by linear speed function for local segmentation with robust initialization and applications in MR brain images. *Signal Processing*, 2014. ISSN 01651684. doi: 10.1016/j.sigpro.2013.10.008.

[97] Li Wang, Chunming Li, Quansen Sun, Deshen Xia, and Chiu-Yen Kao. Active contours driven by local and global intensity fitting energy with application to brain MR image segmentation. *Computerized Medical Imag-*

ing and Graphics, 33(7):520–531, 2009. ISSN 0895-6111. doi: https://doi.org/10.1016/j.compmedimag.2009.04.010.

[98] Wencheng Zhao, Xianze Xu, Yanyan Zhu, and Fengqiu Xu. Active contour model based on local and global Gaussian fitting energy for medical image segmentation. *Optik*, 158:1160–1169, 2018. ISSN 0030-4026. doi: https://doi.org/10.1016/j.ijleo.2018.01.004.

[99] Tao Wang, Irene Cheng, Anup Basu, et al. Fluid vector flow and applications in brain tumor segmentation. *IEEE Transactions on Biomedical Engineering*, 56(3):781–789, 2009.

[100] M Lorenzi, N Ayache, G B Frisoni, and X Pennec. LCC-Demons: A robust and accurate diffeomorphic registration algorithm. *Neuroimage*, 81:470–483, 11 2013. ISSN 1053-8119. doi: 10.1016/j.neuroimage.2013.04.114.

[101] Tim McInerney, Demetri Terzopoulos, Tim McInerney, Demetri Terzopoulos, and Demetri Terzopoulos. Deformable models in medical image analysis: a survey. *Medical image analysis*, 1(2):91–108, 6 1996. ISSN 1361-8415. doi: 10.1016/S1361-8415(96)80007-7.

[102] Alan William Dougherty and Jane You. A kernel-based adaptive fuzzy c-means algorithm for m-fish image segmentation. In *Neural Networks (IJCNN), 2017 International Joint Conference on*, pages 198–205. IEEE, 2017.

[103] Kun He, Dan Wang, and Xu Zhang. Image segmentation using the level set and improved-variation smoothing. *Computer Vision and Image Understanding*, 152:29–40, 2016. ISSN 1090235X. doi: 10.1016/j.cviu.2016.06.006.

[104] Chunming Li, Chenyang Xu, Changfeng Gui, and M.D. Fox. Level Set Evolution without Re-Initialization: A New Variational Formulation. In *2005 IEEE Computer Society Conference on Computer Vision and Pattern Recognition (CVPR'05)*, volume 1, pages 430–436. IEEE, 2005. ISBN 0-7695-2372-2. doi: 10.1109/CVPR.2005.213.

[105] C Li, C Xu, C Gui, and M D Fox. Distance regularized level set evolution and its application to image segmentation. *IEEE Trans Image Process*, 19 (12):3243–3254, 2010. ISSN 10577149. doi: 10.1109/TIP.2010.2069690.